Journal of Materials Chemistry A

REVIEW

View Article Online
View Journal | View Issue

Cite this: J. Mater. Chem. A, 2023, 11, 22656

Recent advances in synthesis of water-stable metal halide perovskites and photocatalytic applications†

He Zhao, [a] Krisztian Kordas*[b] and Satu Ojala *[a]

Solar-driven photocatalytic reactions have attracted wide interest as a viable method to generate green energy and alleviate environmental challenges posed by fossil fuels. Although, various classes of photocatalysts have been explored during the past decades, the pursuit towards even more efficient ones is still ongoing. Metal halide perovskites (MHPs) have been recently proposed as novel photocatalysts owing to their wide light absorption range and excellent optoelectronic properties. However, the instability of MHPs in water is the main obstacle that impedes their applications in practice and prompts stabilization strategies to be developed. This review focuses on the recent approaches for stabilizing MHPs in water, including surface engineering, common-ion effect, and intrinsic water stability. The photocatalytic applications of water-stable MHPs are summarized and an outlook with perspectives over the current challenges are provided.

Received 20th August 2023
Accepted 7th October 2023

DOI: 10.1039/d3ta04994a

rsc.li/materials-a

1 Introduction

During recent years, the exploration of greener energy sources has become of utmost importance to alleviate the inordinate reliance on non-renewable fossil fuel reserves and the consequent serious energy shortage and environmental pollution.[1] Specifically, solar radiation, as an abundant, virtually endless, and green source of energy, has been seen as a promising option for the replacement of fossil fuels.[2] In this context, the question of how to convert solar energy into fuels and value-added chemicals in an efficient and economic manner is a pivotal issue. So far, diverse solar-to-chemical energy conversion systems, including conventional heterogeneous photocatalysis, photoelectrochemical and combined photovoltaic-electrocatalytic systems have been proven to meet the requirements and developed for practical use.[3] Compared with other reported systems, photocatalytic routes are probably the

[a]Environmental and Chemical Engineering Research Unit, Faculty of Technology, University of Oulu, PO Box 4300, FI-90014 Oulu, Finland. E-mail: satu.ojala@oulu.fi
[b]Microelectronics Research Unit, Faculty of Information Technology and Electrical Engineering, University of Oulu, P. O. Box 4500, FI-90014 Oulu, Finland. E-mail: krisztian.kordas@oulu.fi

† Electronic supplementary information (ESI) available. See DOI: https://doi.org/10.1039/d3ta04994a

He Zhao

He Zhao is a doctoral researcher in the Faculty of Technology at the University of Oulu. He received his BSc degree in Materials Chemistry at Zhengzhou University in 2014 and his MSc degree in Materials Physics and Chemistry from Xinjiang Technical Institute of Physics & Chemistry, University of Chinese Academy of Sciences in 2017. His current research interests include lead-free halide perovskites, semiconductor photocatalysis, 2D materials and photocatalytic hydrogen production.

Krisztian Kordas

Krisztian Kordas, MSc Physics and Chemistry (1998, Univ. Szeged), Dr Tech. in Microelectronics, Docent of Nanotechnology, Professor of micro- and nanoelectronic materials and components for ICT applications (2002, 2005, 2016, Univ. Oulu). He has led or participated in more than 20 national and international research projects, published 190+ papers, co-authored 6 book chapters, and supervised 11 doctoral students to graduation. His team's research is focused on synthesis, characterization, and implementation of nanostructured materials for electronics, sensors as well as for energy and environmental applications.

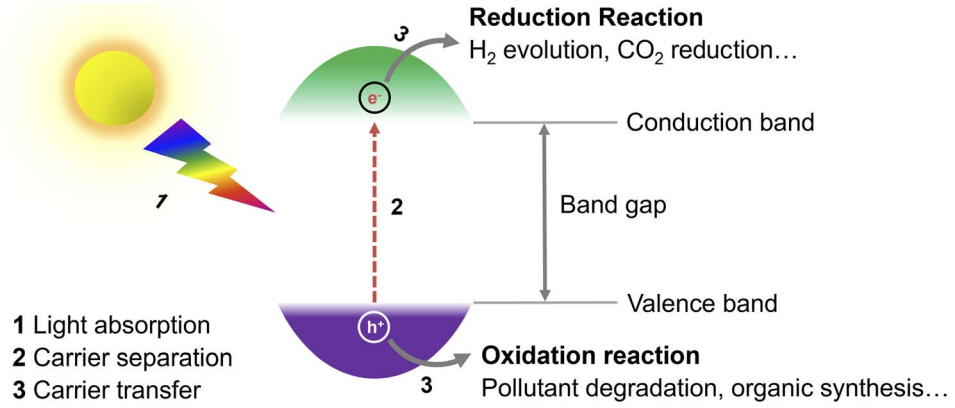

Fig. 1 Basic mechanism of heterogeneous photocatalysis.

simplest ones and easiest to implement. For example, Domen's group has already designed a 100 m^2 array of panel reactors to demonstrate hydrogen evolution from water over several months safely, with a maximum solar-to-hydrogen (STH) energy conversion efficiency of 0.76%.[4] In a recent work of Zhou *et al.*, the efficiency has been improved significantly to 9.2%,[5] which is close to the proposed target for commercialization according to techno-economic analysis.[6] However, compared with the latest 47.6% solar-to-electricity conversion efficiency of the state-of-the-art four-junction solar cells,[7] there is still a long road ahead to achieve such values in photocatalytic systems.

Exploring efficient, stable photocatalysts is thus one vital research field. In photocatalysis, the key component of the process is the photocatalyst (Fig. 1), whose role is to transform solar energy to charge carriers (electrons and holes) after light absorption, which then drift to the surface of the photocatalyst and participate in reduction/oxidation reactions.[8] To date, several different photocatalysts either homogenous or heterogeneous have been proposed,[9] including *e.g.*, transition metal complexes,[10] organic photoredox catalysts,[9] titanium dioxide,[11,12] carbon nitride,[13,14] and perovskites.[15] As most of the so far explored photocatalytic materials suffer from (i) limited photostability, high cost and potential toxicity,[16] (ii) narrow utilizable solar spectral absorption range,[17] (iii) sluggish charge carrier transport from the bulk of a photocatalyst to the surface and/or (iv) fast charge carrier recombination,[11] there is a room to improve conversion efficiencies.[18,19]

The family of metal halide perovskites (MHPs) appears to offer features that tackle the aforementioned issues simultaneously. Organolead trihalide perovskites (*e.g.*, $CH_3NH_3PbI_3$) have emerged as novel high-performance photoactive absorbers with rocketing power conversion efficiency from 3.8% to certified 25.5% in just a few years.[20,21] In general, the remarkable photovoltaic performance of MHPs originates from their high absorption coefficients,[22,23] wide absorption window,[20] long electron–hole diffusion lengths[22,24] and high carrier mobility.[25] All these excellent optical and charge-transport characteristics predestinate MHPs as ideal candidates for photocatalytic processes.[26] However, every coin has two sides, and unfortunately MHPs are not exceptions either. The ionic nature of MHPs imparts their vulnerability toward moisture and polar solvents (especially water), which severely restricts their photocatalytic applications,[27] and remains to be resolved. In 2016, Park *et al.* reported the pioneering work concerning the stabilization of $CH_3NH_3PbI_3$ ($MAPbI_3$) in aqueous HI solution by exploiting the common-ion effect; however, this happens under harsh conditions, at pH < −0.5 and $-\log[I^-] < -0.4$.[28] Nevertheless, environmental concerns, costs, and the demand for practical conditions necessitate photocatalytic processes to be performed preferably in aqueous systems having less extreme chemistries.[29] While MHP-based photocatalysts have been reviewed from different perspectives, such as photoredox organic synthesis,[30–33] CO_2 reduction,[34–39] and H_2 generation,[40–47] strategies to synthesize water stable MHPs or their photocatalytic applications are not yet adequately summarized. Therefore, in this review, we survey and overview the recent progress in stabilizing MHPs against water, and discuss the encountered challenges and potential limitations of their applications, with the goal of providing new ideas and inspiration to advance the design new generations of efficient MHP-based photocatalytic systems.

Satu Ojala

Satu Ojala gained her MSc in Chemical Engineering in 2000 and DSc (Tech) in Environmental Engineering in 2005 with Distinction from the University of Oulu, Finland. She worked as a postdoc at the University of Poitiers, France between 2006 and 2007, and at VTT Technology Research Center between 2008 and 2013. She gained her adjunct professorship in 2012 in the field of Environmental Catalysis from the University of Oulu. Her main field of research is Environmental Engineering, especially heterogeneous catalytic processes in gas and liquid phases. She has a special interest in in situ and operando spectroscopy applied in catalysis research.

2 Stabilization methods

Conventional lead-based MHPs are prone to decompose when exposed to moisture. It is reported that the perovskite solar cells lose more than 80% of their initial efficiency after one-day storage in ambient air, and only 5% is retained after 6 days.[48] Encapsulation of the MHP films using materials having diffusion barrier properties have been proposed to protect the MHP solar cells from moisture hence maintaining more than 90% of their initial performance for almost 2 months.[49] This is still far from the commercial long-term stability expected (25 years is typical for silicon solar cells),[50] thus the challenge in the MHP development remains to be solved.

To improve the water stability of MHPs, the role of water in the degradation of MHPs needs to be elucidated. The published results indicate that the MHPs adsorb water molecules quickly with a time scale of seconds[51] and a single water molecule can accelerate the degradation of perovskite *via* acid–base reaction.[52] What is even more troublesome, is that the water intake is not limited only to surface adsorption, but the water molecules also diffuse and penetrate the bulk and even infiltrate the $MAPbI_3$ unit cells (Fig. 2). However, some studies claim that MHPs have a minor tolerance to water. For example, $MAPbI_3$ was reported to remain intact when exposed to below 2×10^{10} Langmuir of H_2O (one Langmuir equals to an exposure of about 1.33×10^{-4} Pa for one second).[53] Only ~1% volume expansion of the crystal structure is observed although water incorporated in the perovskite.[54] These results are consistent with previous reports of a reversible process between the hydration and dehydration stages of $MAPbI_3$.[55,56] To figure out the detailed degradation mechanism under moist conditions, the dependence of spatially resolved external quantum efficiency (EQE) under various humidity exposure conditions has been investigated by using laser beam induced current mapping, and a four-stage degradation process has been proposed.[57] When a tiny amount of water (1.6% H_2O in N_2) is introduced and kept for a short time (6 min), EQE increases marginally and reaches a maximum, which is caused by the solvation of $CH_3NH_3^+$ (MA^+) and I^- ions,[58] that heals some defects, reduces the trap density, and thus improves the uniformity of perovskite films (Stage 1). As the time increases, a slow drop in EQE is observed due to the change of the electronic structure and carrier mobility of hole-transporting materials (Stage 2). In the next stage (Stage 3), a sharp decrease of EQE indicates the breakdown of 3D structure, while monohydrated 1-dimensional (1D) chains of $CH_3NH_3PbI_3 \cdot H_2O$ or 0-dimensional (0D) dots of dihydrates $(CH_3NH_3)_4PbI_6 \cdot 2H_2O$ are formed (Stage 3). Finally, the degradation of MHPs results in the formation of CH_3NH_3I (MAI), PbI_2 and water (Stage 4). In general, the decomposition starts at the surface, especially at the MAI-terminations.[54] The loss of MA^+ results in an open inorganic framework to form vacancies inside the crystal lattice that finally leads to a rapid deterioration or decomposition of the perovskite structure.[59] The dissolution of I^- ions in water is easier than that of MA^+ ions since the hydrophobicity of $-CH_3$ group in MA^+ requires higher dissolution energy.[60] These studies indicate that water molecules penetrate easily into the bulk of MHPs and the removal of ions (especially the I^- ions due to the lower energy barrier) is the main cause of the degradation. Based on the observations above, thus, the main strategies to obtain water stable MHPs are: (i) preventing the structure from the contact of water, (ii) compensating for the depletion of ions from the surrounding, and (iii) reducing the solubility of organic cations. In these efforts, three different strategies have been proposed, including surface engineering, utilization of the common-ion effect, and enhancement of the intrinsic stability of perovskites.

2.1 Surface engineering

Surface engineering has been explored to generate protecting layers on the MHPs, thus avoiding the direct contact of water with MHPs. In this section, six surface passivation methods are discussed: (1) organic ligands, (2) organic polymers, (3) inorganic materials, (4) metal–organic frameworks (MOFs), (5) phase engineering, and (6) water-assisted engineering.

2.1.1 Organic ligands. The application of organic ligands is a well-established strategy to manipulate the shape and size of

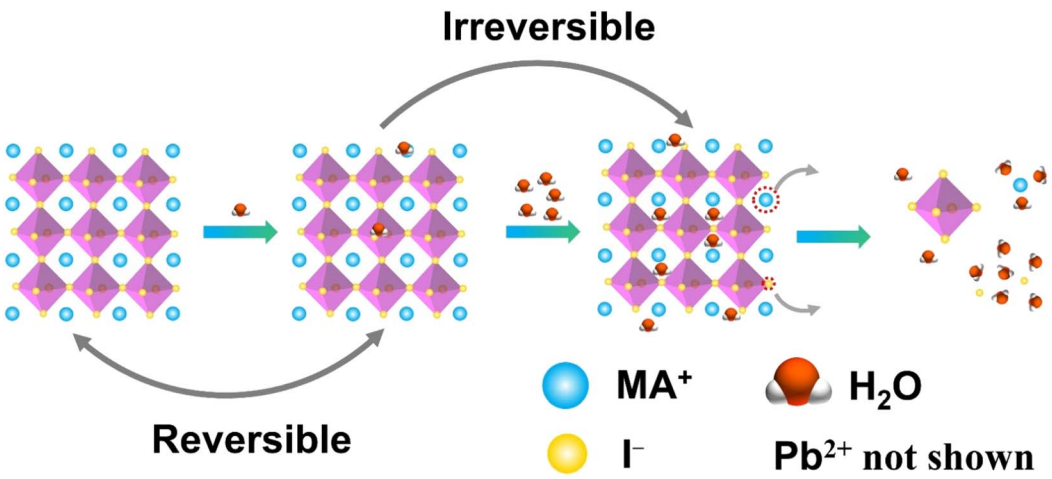

Fig. 2 Schematic illustration of $MAPbI_3$ decomposition in water.

MHP nanocrystals (NCs),[61] and also to stabilize MHPs.[62] Normally, frequently used ligands in synthesis of MHP NCs are oleic acid (OA) and oleylamine (OAm), which improve the dispersion of MHP NCs in nonpolar solvents, such as toluene and hexane. However, the dynamic adsorption–desorption process between the ligands and MHP NCs render the easy detachment[63] and removal of ligands in proton-donating solvents, causing the degradation of MHP NCs,[64] and consequent deterioration of their luminescent properties (including the electron density of states of emission bands, and the photoluminescence quantum yield).

The introduction of hydrophobic ligands on the surface of MHPs is one of the most efficient and convenient approaches to stabilize MHPs. A post-surface functionalization with hydrophobic cations *via* simple ligand exchange process can substitute surface methylammonium (MA^+) ions and enhance the stability of MHPs. Many studies have indicated that the presence of hydrophobic quaternary ammonium cations, such as tetra-methyl ammonium, $(CH_3)_4N^+$;[65–67] tetra-ethyl ammonium, $(C_2H_5)_4N^+$;[68] tetra-butyl ammonium, $(C_4H_9)_4N^+$;[69,70] and tetra-hexyl ammonium, $(C_6H_{13})_4N^+$;[71] have a vital influence on the moisture-stability of MHPs. These quaternary ammonium cations adsorb chemically on the surface of MHPs, and inhibit the water intake of the lattice thus keeping the perovskite films stable under 90 ± 5% relative humidity (RH) for more than 30 days without a photovoltaic loss. This happens because the bulky organic cations shift the surface Pb_{5C}–I_{1c} (I_{1c} represents the surface I atom coordinated with one Pb atom) bonds owing to the steric effects and impede the water adsorption on the five-coordinated surface Pb atoms (Pb_{5c}).[71] In addition, these molecules can also suppress the iodide migration,[72] evidenced by the shortened Pb–I bond (from 3.17 Å to 3.07 Å, Fig. 3a). Besides these factors, the formation of water-stable quaternary ammonium lead iodide shell may also contribute to the enhanced stability.[66,73,74] For example, with $(C_4H_9)_4NI$ post-treatment over $CsPbI_3$, the $(C_4H_9)_4N^+$ cations can intercalate the inorganic framework of MHP and exchange Cs^+ ions, forming a one-dimensional $(C_4H_9)_4NPbI_3$ layer[75] exhibiting intrinsic water stability (Fig. 3b).[76]

Sufficient interactions between MHPs and ligands should also be considered because the instability MHP NCs partly originates from the easy detachment of ligands as described above.[77] Clearly, introducing reactive groups in the capping ligands and forming a covalent or ionic bonding between ligands and MHPs are deemed to improve the water stability of MHPs. For example, polyhedral oligomeric silsesquioxane (POSS) having a mercaptopropyl anchor group attaches to the surface of MHP NCs and forms a cage-like structure. Such POSS-protected $CsPbX_3$ (X = Br and/or I) NCs were shown to maintain the original green light emission and stability in water for 10 weeks.[78] Unlike the physical encapsulation strategy with hydrocarbons,[79,80] the impressive enhancement of water

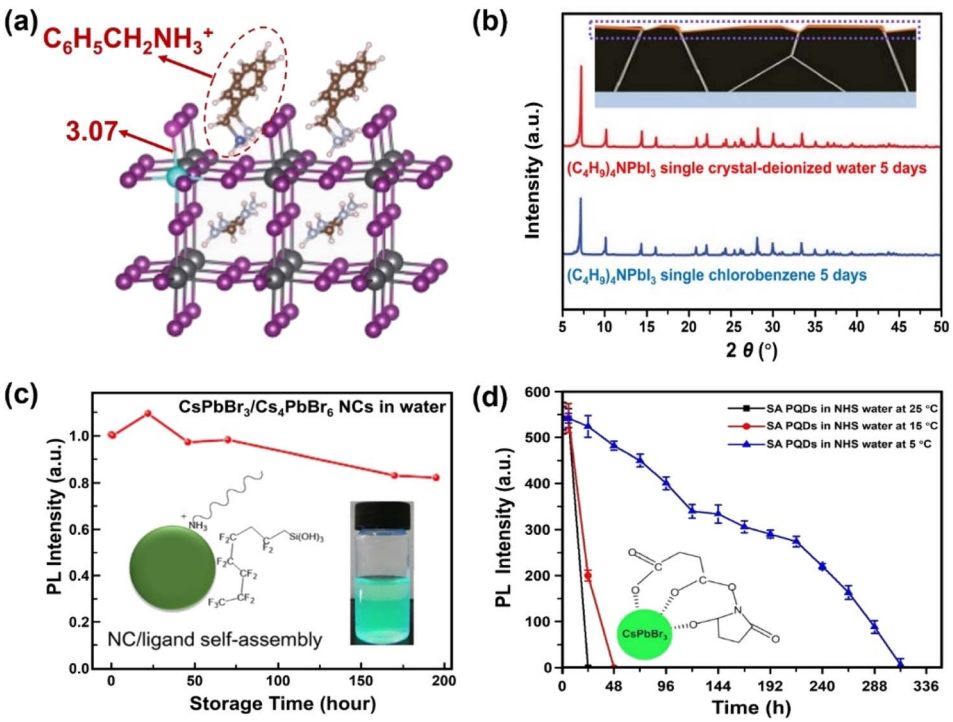

Fig. 3 Ligand engineering for water-stable MHPs. (a) Length of Pb–I bond over $FA_{0.83}Cs_{0.17}PbI_3$ after adding phenylmethylammonium ions. Adapted from ref. 72. (b) Formation of $(C_4H_9)_4NPbI_3$ layers over MHP from a $(C_4H_9)_4NI$ post-treatment and XRD patterns of $(C_4H_9)_4NPbI_3$ single crystals after 5 days immersion in water and toluene. Adapted from ref. 76. Copyright 2021 John Wiley and Sons. (c) Variations of PL intensity over fluorocarbon-coating $CsPbBr_3/Cs_4PbBr_6$ NCs in water. Adapted from ref. 86. Copyright 2018 American Chemical Society. (d) PL intensity evolution of succinic acid-capping $CsPbBr_3$ QDs in *N*-hydroxy succinimide water and the formation of tridentate ligands over QDs. Adapted from ref. 93. Copyright 2021 Elsevier.

stability results from the strong metal–thiol interactions between POSS and MHPs.[81,82]

Compared with metal–thiol interaction, the fluorine in fluorocarbons is expected to form a stronger interaction with MHPs owing to its high electronegativity.[83] The fluorocarbon agents (FCAs) have a low surface energy, featuring superior hydrophobicity compared to the corresponding hydrocarbons.[84] In addition, the abundance of $-CF_2-$ and $-CF_3$ groups and the amphiphilic nature trigger the self-assembly in aqueous solution.[85] As an example, after coating with FCAs ($(C_6F_{13}CH_2CH_2Si(OCH_2CH_3)_3$, $C_6F_{13}CH_2CH_2OOCCH{=}CH_2$, $C_6F_6H_7Si(OCH_2CH_3)_3$ or $C_3F_6CH_2CH_2OOCCH{=}CH_2)$), the $CsPbBr_3/Cs_4PbBr_6$ NCs exhibited a high absolute photoluminescence quantum yield (PLQY) of ~80% in water for weeks as expected (Fig. 3c). Because of their excellent performance, short fluorocarbon chains (down to C4) of FACs are also able to stabilize the perovskite NCs in water. After additional coating with $BaSO_4$, the $CsPbBr_3/Cs_4PbBr_6/BaSO_4$ NCs retain 90% of the initial fluorescence intensity after 1 day storage at room temperature in saline solution, which broadens the potential applications in biology.[86] Among the above FCAs, $C_3F_6CH_2CH_2OOCCH{=}CH_2$ can be further transformed to amphiphilic hexafluorobutanol (HFBO) with a polar C–OH head in the presence of water resulting in good water solubility and long-term stability in aqueous solution for more than 100 hours.[87] The concentrated hydroxyl ligands may also serve as a water-proof layer to avoid further water attack.[88]

Efforts to explore ligands with dual functions, namely, hydrophobicity and bonding property, have been also extended to metal stearates (*e.g.*, $AlSt_3$, $ZnSt_2$, NaSt). The long carbon chains protect MHPs from the surrounding environment, meanwhile, the coordinate bonding of St–Pb,[89] St–Cs[90] or ionic bonding of Al^{3+}–Br^- also provides a stronger interaction than the van der Waals bonds between OA (or OAm) and MHPs. The $CsPbBr_3$-$AlSt_3$ nanocomposite suspension exhibited bright photoluminescence (PL) after 25 min sonication in water or overnight storage[91] and excellent stability in water for more than 60 days.[92]

However, introducing long chain ligands on the surface of MHPs usually deteriorates the charge transfer from MHPs to the coating and the adsorption of reactants, which is unfavorable to the photocatalytic activity.[95–100] It is found that the employment of short chain ligands over NCs or QDs can enhance charge transfer rate[101,102] and subsequently improve the photocatalytic activity of $CsPbBr_3$ NCs.[103] These findings indicate that utilizing short chain ligands is an exciting means for improving the stabilization of the MHPs without a compromised charge mobility. Up to now, a series of short chain multidentate ligands have been explored, which can be classified as acids (succinic acid,[93] 2,2′-iminodibenzoic acid,[104] 4-mercaptobenzoic acid,[105] octadecanedioic acid[106,107]), amino acids (aminocaproic acid[108]), pyridines (2,2′-bipyridine, 2,2′:6′,2″-terpyridine,[109] 2-mercaptopyridine[107,110,111]), salts (potassium dichloroacetate,[112] N1,N2-didodecyl-N1,N1,N2,N2-tetramethylethane-1,2-diaminium bromide[113]), and zwitterions.[114] One example is succinic acid, which has two carboxylic acid groups. After coupling with $CsPbBr_3$ QDs, the composites exhibit enhanced water-stability because of the improved crystallinity and stronger bonding with $CsPbBr_3$ QDs.[93] Further activating the carboxyl groups with *N*-hydroxy succinimide (NHS) in water would form a tridentate ligand over $CsPbBr_3$ QDs as depicted in Fig. 3d. The light emission over the composites lasts for 24 h and 48 h at 25 °C and 15 °C, respectively, and expands to two weeks at 5 °C. The reviewed various ligand strategies and their water stabilities are summarized in Table 1.

2.1.2 Organic polymers. Polymer-based coating materials have several merits, such as solution processability, mechanical performance, and chemical functionalization. More importantly, polymers with abundant functional groups are good candidates to bond with surface ions of MHPs, improving both PLQYs and stability simultaneously[115–117] without compromising light absorption.[118] In addition, polymer matrices are capable of water uptake *via* water-induced swelling process[119] and thus alleviate the direct contact of water and MHPs to a degree.[120]

Photopolymers, such as Norland Optical Adhesive (NOA) 63,[121] NOA 61,[7] and Ergo® optical adhesive 8500 (Ergo),[122] have been exploited firstly to stabilize MHPs because of their popularity in optoelectronic devices. They are polyurethane-related polymers, which can form crosslinked networks quickly upon UV curing. For instance, the Ergo-coated $CsPbBr_{0.6}I_{2.4}$ film maintained 91% PL intensity after soaking in water for 24 hours with only 6% loss of PLQY. Although the photocuring process improves the robustness of MHPs,[123] this physical blending strategy may cause heterogeneous phase aggregation and can lead to instability.[124] This is because of the specific surface area and volume effects of MHP NCs[125] as well as the large difference in polarity of perovskites and polymers.[126]

In contrast to ligand modifications occurred on the surface of MHPs, most polymer–MHP NC composites have been produced by swelling–deswelling process of polymers. During the dynamic process,[127] the dissolved solutes (mainly MHP's precursors) can penetrate into the polymer and the MHPs then grow inside the 3D network of polymer, after which the polymer shrinks during solvent evaporation or the addition of theta solvent. Therefore, MHPs become confined within the polymer thus limiting their contact with the surrounding environment. One important parameter to be optimized for such composites is the ratio of polymer and MHP constituents. Too small amounts of the polymer phase lead to insufficient protection and consequent degradation, whereas the other extreme results in turbid mixtures. As one example, the ratio of poly(isobutylene-alt-maleic anhydride)-*graft*-dodecyl (PMA) and MHP NCs showed a significant effect on the final water stability of the composites. It is found that the polymer-to-nanoparticle ratio ($R_{pol/area}$, number of monomers of polymer per nanoparticle area [nm^2]) should be controlled in the range of 1000–3000. $CsPbBr_3$ NCs-PMA composites with a $R_{pol/area}$ of 1500 show good water stability for at least 8 months.[128] The ratio also seems to influence the PL intensity of the composites. Too high MHP NC content will reduce the PL intensity due to the fluorescence self-quenching of NCs.[124]

Besides the molar ratio, the chemical structure of polymer also dominates the stability. Many polymers have been

Table 1 Summary of ligand strategies for the synthesis of water-stable MHPs

Water-stable MHPs		Stability					
Materials	Method of preparation	Medium	Characterizations	Retained PL intensity	PLQY before (after)	Observed durability	Ref.
$(C_4H_9)_4NPbI_3$	Solvent evaporation	Water (immersion)	PXRD	—	—	5 days	76
NBCAnPbI$_3$/$CH_3NH_3PbI_3$	Precipitation	Water (immersion)	UV-vis absorption spectroscopy PXRD	—	—	30 min	73
Paraffin-$CsPbX_3$	Physical blending	Water (immersion)	PL	78%		20 days	79
Paraffin-$CsPb_{0.7}Sn_{0.3}Br_2I$ QDs	Physical blending	Water (immersion)	PL	—	—	20 days	80
POSS-$CsPbBr_3$	Physical blending	Water (suspension)	PL	—	62% (—)	10 weeks	78
POSS-$CsPb(Br/I)_3$	Physical blending	Water (immersion)	PL	—	45% (—)	10 weeks	78
PFOTHS-$CsPbBr_3$/Cs_4PbBr_6 NCs	Aqueous synthesis	Water (suspension)	PL	>80%	79.2% (—)	200 h	86
PFOTHS-$CsPbBr_3$/Cs_4PbBr_6/$BaSO_4$	Aqueous synthesis	Saline solution (suspension)	PL	90%	—	1 day	86
Hexafluorobutyl methacrylate-coated $Co_{2\%}$@$CsPbBr_3$/Cs_4PbBr_6 NCs	Physical blending	Water (suspension)	PL	>90%	~80% (—)	100 h	87
$CsPbBr_3$-$AlSt_3$ NCs	Physical blending	Toluene/water (floating)	PL	—	—	Overnight	91
$CsPbBr_3$-$AlSt_3$ QDs	Co-precipitation	Water (suspension)	PL	~100%	—	60 days	92
Succinic acid-capped $CsPbBr_3$ QDs	Ligand exchange	Toluene/water (suspension)	PL	85%	—	—	93
Succinic acid-capped $CsPbBr_3$ QDs in NHS water	Ligand exchange and physical blending	Toluene/water 5 °C (suspension)	PL	—	—	312 h	93
SLNs-$CsPbBr_3$	Sonication-assisted melt homogenization	Water (suspension)	PL	—	13% (—)	2 months	94
SLNs-$CsPb(Br_{0.2}I_{0.8})_3$	Sonication-assisted melt homogenization	Water (suspension)	PL	—	9% (—)	2 months	94

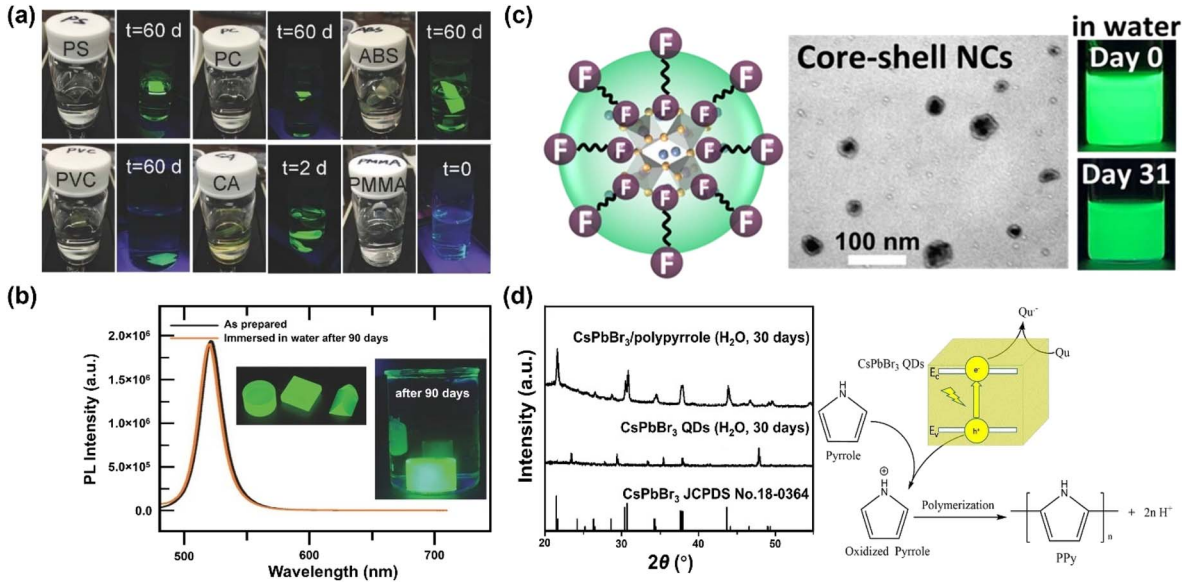

Fig. 4 Polymer encapsulation over MHPs. (a) Fluorescent photos of polystyrene, polycarbonate, acrylonitrile butadiene styrene, cellulose acetate and poly(methyl methacrylate)–$MAPbBr_3$ composites at different periods. Adapted from ref. 129. Copyright 2016 John Wiley and Sons. (b) Comparison of PL spectra over $MAPbBr_3$ NC–V18 composites before and after a 90 days immersion in water. Adapted from ref. 133. Copyright 2017 John Wiley and Sons. (c) TEM image and photos of $CsPbBr_3/Cs_4PbBr_6$ NCs protected by fluoropolymer shell. Adapted from ref. 138. Copyright 2022 American Chemical Society. (d) Visible light photopolymerization synthesis of $CsPbBr_3$/polypyrrole composites and XRD patterns after 30 days water immersion. Adapted from ref. 145. Copyright 2020 Elsevier.

examined as hosts, including polystyrene (PS), polycarbonate (PC), acrylonitrile butadiene styrene (ABS), cellulose acetate (CA), polyvinyl chloride (PVC), poly(methyl methacrylate) (PMMA) and poly(styrene/acrylamide).[129] Among those, PS, PC, PVC and ABS can protect MHP NCs from being attacked by water for periods of months, while the CA loses stability after two days, and PMMA-protected MHP NCs fail instantly (Fig. 4a). The failure of CA originates from its hydrophilic character and thus its high-water permeability, whereas the reason of PMMA is likely stemming from its low swelling ratio of PMMA in DMF solvent and weak bonding interaction with MHPs. Specifically, the $MAPbBr_3$–PS and $MAPbBr_3$–PC composite films can survive in boiling water for 30 min with less than 15% and 7% of decay in PLQY, respectively.[129] The protecting effect of crosslinked PS is much better than other uncross-linked polymers because it cannot swell in polar solvents. For instance, the $CsPbBr_3$@PS composites maintain 65.7% of the absolute PLQYs after stirring in water for 3 days, and still exhibit strong green luminescence after 9 months storage.[130] Note that the composites have a good stability in acid/alkali aqueous solution, and even biologic buffers, showing advantages in monitoring pH, urea, and urease.[131]

Usually, the dissolution or swelling of polymers is time-consuming, especially for those of high-molecular-weight. Hence, the MHPs need to be prepared prior to coupling; however, serious degradation or aggregation may occur during the storage of MHP NCs or QDs. Through adding crosslinkable monomers into the MHP's precursor solution, polymer–MHPs composites can be achieved in a one-pot reaction assisted by heating or UV irradiation.[132] For example, a crosslinked 4-vinylbenzyl-dimethyloctadecylammonium chloride (V18)-$MAPbBr_3$ NC composite has been prepared *via in situ* polymerization under 90 °C for 30 min by employing azobisisobutyronitrile (AIBN) as an initiator.[133] The crosslinked $MAPbBr_3$ NC–V18 retains about 85% of PL intensity after immersion in water for 120 min. After copolymerization with methyl methacrylate, the water-resistance extends to 90 days without the change of its PL (Fig. 4b). However, the decomposition products of remaining photo-initiator may have an unintended consequence on the property of polymers and MHPs.[147] The alternative approach is to utilize polymers (for example, copolymer micelles) as nanoreactors and grow the MHPs inside the polymers. In contrast to random growth of MHPs during swelling–deswelling process, block copolymer micelles are highly ordered structures, featuring superior size uniformity and high stability of individual micellar building blocks, which are often employed as templates and scaffolds for producing arrays and ordered structures of nanomaterials.[134,148,149] One good example is employing polystyrene-poly(2-vinlypyridine) (PS-*b*-P2VP) diblock copolymer micelles as nanoreactors to prepare monodisperse polymer–MHP NCs. The resultant composites display strong stability against water over 75 days.[134]

Similar to the strategies with ligands, improving the interface interactions between MHPs and polymers by introducing anchoring groups, such as –COOH groups[139,150] and $-CF_2$ groups,[136] can enhance the stability of polymer–MHPs.[151] For example, PMMA has been widely used as passivation to protect solar cells from oxygen and moisture.[152–154] On the other hand, it fails to stabilize MHPs in water owing to the too weak interaction between those. Jiang *et al.* found that partially hydrolyzing

PMMA (below 10%, h-PMMA) would form methacrylic acid anchors in PMMA chain.[137,150] These anchors work as ligands and enhance the PMMA–MHP interaction, thus improving the water stability. Thus, a good interaction between the MHPs and polymers is a prerequisite to the success of good stability. For example, a fluoropolymer (Hyflon) was used to stabilize $CsPbBr_3/Cs_4PbBr_6$ NCs and it was found that the CF_2 groups from Hyflon are strongly bonded on the surface of MHPs (Fig. 4c), forming a ligand shell over $CsPbBr_3/Cs_4PbBr_6$ NCs core having good stability for at least one month.[138]

The strength of interaction at the polymer–MHP interface is also influenced by the compatibility of surface organic ligands on MHPs and hydrophobic polymers.[155] For instance, OA and OAm ligands capped MHP particles can be stabilized by polymers having long alkyl chain ligands because the similar alkyl chains has a good compatibility and thus create a better MHP–polymer interface.[143] Introducing interfacial layers (*e.g.*, polyvinyl pyrrolidone, PVP) can not only serve as an additional barrier, but also improve the compatibility of MHP with polymer matrix. For PVP, it is a widely used coupling agent. Owing to the amphiphilic characteristics, PVP can be adsorbed on different surfaces, including metals, metal oxides, polymers (*e.g.*, PS, cellulose).[156] Inspired by this, PVP has been employed serving as an effective interfacial layer between MHP NCs and polymer for the design of water-stable MHPs.[140,141] Similar to the multidentate ligands, block copolymers have inherently different domains and provide more functional features. As an example, polystyrene-*block*-poly(ethylene-ran-butylene)-*block*-polystyrene (PS-PEB-PS) and poly(ethylene glycol)-*block*-poly(-propylene glycol)-*block*-poly(ethylene glycol) (PEG-PPG-PEG) have been applied to encapsulate the $CsPbBr_3$ QDs. The obtained nanocomposites display luminescence in water for 8 days.[142] The results suggested that the PS blocks interact with the hydrophobic parts (surface ligands) of QDs; the PEG moiety, as Lewis base, would have a strong interaction with Lewis acid ($PbBr_2$) and acts as water protection barrier.[182]

In addition to the interfacial interaction, the thickness of coating also has a significant effect on water-resistance.[183] While thicker coatings provide better stability, those can seriously compromise charge transport (tunneling), when the coating thickness exceeds a few nanometers.[184,185] Thus, tailoring the thickness to balance the water-resistance and charge transportation is necessary. By chemical crosslinking the polymer chains, a thinner dense covalent-bonded 3D polymer network can be formed. Therefore, molecules having multiple sites for crosslinking, such as, 2-((acryloyloxy)methyl)-2-(((12-guanidinododecanoyl)oxy)methyl)propane-1,3-diyl diacrylate (PETA-G) can be polymerized efficiently to provide a sufficiently thin shell around MHPs without compromising the charge transport property.[144]

Based on the above analysis, polymers offer a good strategy to form protecting layers on MHPs for stabilization. However, in most cases, their limited electrical transport properties impede the extraction and transfer of charge, and consequently can compromise their applications in photocatalysis and photoelectrocatalysis. To overcome such limitations, polymers having conjugated electronic structure (*e.g.*, polypyrrole and polyaniline) and hence reasonable charge transport properties (typically *via* hopping mechanisms) have been applied.[186] As shown in Fig. 4d, the composites exhibit dramatic enhancement of water stability as well as improved charge transport behavior.[145,146] Unfortunately, these conducting polymers also suffer from limited stability especially in O_2 and water, caused by doping effects and also by the electroactive nature of such polymers.[187,188]

Accordingly, to build a successful strategy to produce water-stable polymer coated MHPs (Table 2), simultaneously, several aspects of materials selection and synthetic routes shall be considered (Fig. 5).

2.1.3 Inorganic materials. Compared to organic ligands/coatings, stabilization and passivation of MHPs with inorganic materials (*e.g.*, Al_2O_3, SiO_2, TiO_2, ZrO_2) offer airtight and mechanically more robust alternatives.[189]

For coatings with a thin Al_2O_3 layer, trimethylaluminum (TMA) vapor-based atomic layer deposition (ALD) has been reported to form covalent bonds with MHP NCs.[190] The ALD is emerging as a useful method for depositing thin films with excellent conformality, uniformity, precise thickness control and high quality. Considering that it can be carried out at moderate temperatures,[191] the technique is particularly attractive to coat MHPs. Amorphous alumina (AlO_x) encapsulated $CsPbX_3$ QDs have shown improved stability for at least 1 hour.[157] The short stability in water originates from the intrinsic instability of this amorphous overcoat. The stability can be further improved (up to one month) by increasing the growth temperature and hence the crystallinity of alumina on $CsPbBr_3$ nanoplates, as shown in Fig. 6a.[158]

Silicon oxide (SiO_2) is another attractive coating material, featuring good chemical stability, blocking of moisture and oxygen, and excellent transparency. It has been selected as protecting layers for the stabilization of carbon dots,[192] and metal nanoparticles[193] among others. Silica-based mesoporous aerogels (AGs) have been developed as matrix owing to high porosity, large specific surface area, low density and thermal conductivity.[194] The hydrophobic property can be tailored by grafting hydrophobic functional groups over SiO_2 or directly using the silica precursor holding hydrophobic groups. Diverse types of pores (micropore, mesopore and macropore) can host the $CsPbBr_3$ QDs and supply enhanced water stability for more than two weeks in hydrophobic AG.[162] However, the polydisperse pores also bring the potential aggregation of MHP QDs. A fine control over the pore size of mesoporous silica will ease the uniform distribution of MHP QDs in random-distributed AGs because of the compatibility of pore size and QDs' mean size[195] and excellent adsorption of QDs on the hydrophobic surface. For example, Li *et al.* have encapsulated the QDs into superhydrophobic aerogel inorganic matrix (S-AIM) with open structures.[163] The composites preserved their initial PL intensity after 11 days of soaking in water (Fig. 6b) and achieved a relatively high PLQY stability (50.5%) after soaking for 3.5 months. This good stability without the sealing of open structure may originate from the matched size between the pore and the particle, the super-hydrophobicity

Table 2 Water-stable MHPs obtained from polymer coatings[a]

Water-stable MHPs		Stability					
Materials	Methods	Medium	Characterizations	Retained PL intensity	PLQY before (after)	Observed durability	Ref.
NOA61/$CH_3NH_3PbBr_3$/glass	Photocurring	Water (washing)	PL	~100%	—	Four cycles	7
$CsPbBr_{0.6}I_{2.4}$ QD/Ergo films	Photocurring	Water (immersion)	PL	91%	43% (—)	24 h	122
$MAPbBr_3$/PMSR (1.13 wt%)	Physical blending	Water (immersion)	PL	93%	53% (—)	576 h	124
$MAPbBr_3$/PMSR (1.13 wt%)	Physical blending	Water (immersion, 70 °C)	PL	91%	53% (—)	50 min	124
$MAPbBr_3$/PMSR (1.13 wt%)	Physical blending	Water (immersion, 100 °C)	PL	77%	53% (—)	20 min	124
$MAPbBr_3$/SSDC (1.13 wt%)	Physical blending	Water	PL	77%	62% (—)	36 h	124
$MAPbBr_3$/SSDC (1.13 wt%)	Physical blending	Water (immersion, 70 °C)	PL	52%	62% (—)	10 min	124
$MAPbBr_3$/SSDC (1.13 wt%)	Physical blending	Water (immersion, 100 °C)	PL	44%	62% (—)	10 min	124
$CsPbBr_3$ NCs-PMA ($R_{pol/area}$ of 1500)	Physical blending	Water (immersion)	PL	—	—	>8 months	128
$MAPbBr_3$–polystyrene	Swelling–deswelling microencapsulation	Water (immersion)	PL	—	34% (32%)	2 months	129
$MAPbBr_3$–polycarbonate	Swelling–deswelling microencapsulation	Water (immersion)	PL	—	31% (31%)	2 months	129
$MAPbBr_3$–acrylonitrile butadiene	Swelling–deswelling microencapsulation	Water (immersion)	PL	—	48% (45%)	2 months	129
$MAPbBr_3$–polyvinyl chloride	Swelling–deswelling microencapsulation	Water (immersion)	PL	—	16% (15%)	2 months	129
$MAPbBr_3$–cellulose acetate	Swelling–deswelling microencapsulation	Water (immersion)	PL	—	47% (—)	2 months	129
$MAPbBr_3$–cellulose acetate	Swelling–deswelling microencapsulation	Water (immersion)	PL	5%	—	48 h	129
$MAPbBr_3$–poly(methyl methacrylate)	Swelling–deswelling microencapsulation	Water (immersion)	PL	—	14% (—)	2 months	129
$MAPbBr_3$–polystyrene	Swelling–deswelling microencapsulation	Boiling water (immersion)	PL	—	34% (29%)	30 min	129
$MAPbBr_3$–polyvinyl chloride	Swelling–deswelling microencapsulation	Boiling water (immersion)	PL	—	31% (29%)	30 min	129
$CsPbBr_3$ QDs@polystyrene	Swelling–shrinking	Water (immersion, stirring)	PL	—	68% (64.7%)	3 days	130
$CsPbBr_3$ QDs@polystyrene	Swelling–shrinking	Water (immersion, stirring)	PL	20–30%	68% (—)	30 days	130
$CsPbBr_3$–poly(methyl methacrylate)	One-pot thermal and UV polymerization	Water (immersion)	PL	54%	54.6% (—)	48 h (30 days)	132
$CsPbBr_3$–poly(butyl methacrylate)	One-pot thermal and UV polymerization	Water (immersion)	PL	56%	62.2% (—)	48 h (30 days)	132
$MAPbX_3$ NCs-polystyrene-poly(2-vinlypyridine) (PS-*b*-P2VP)	*In situ* growth	Water (immersion)	PL	—	—	75 days	134
Polyimide-coated $CsPbBr_3$ NCs	*In situ* growth	Water (immersion)	PL	~80%	88.1% (—)	60 min	135
$MAPbBr_3$ (8 wt%) NCs/polyvinylidene fluoride	*In situ* growth	Water (immersion)	PL	—	94.6 ± 1% (68.1 ± 1%)	400 h	136

Table 2 (*Contd.*)

Water-stable MHPs		Stability					
Materials	Methods	Medium	Characterizations	Retained PL intensity	PLQY before (after)	Observed durability	Ref.
Hydrolyzed poly(methyl methacrylate)-coated $CH_3NH_3PbBr_3$	Mechanical grinding	Water (suspension)	PL	~80%	—	40 days	137
$CsPbBr_3/Cs_4PbBr_6$ NCs-Hyflon-DFTHS/OLA	Physical blending	Water (suspension)	PL	68%	73% (—)	31 days	138
$CsPbBr_3$/octylamine-modified polyacrylic acid + OAm NCs	Ligand engineering	Water (suspension)	PL	80.13%	—	15 days	139
PVP-capped $CsPbX_3$ NCs@polystyrene microhemispheres	Self-assembly	Water (washing)	PL	—	—	3 times	140
Silicone resin/PVP-$CsPbBr_3$ nanofibrous membranes	One-step electrospun	Water (immersion)	PL	—	—	Several hours	141
PS-PEB-PS and PEG-PPG-PEG coated $CsPbBr_3$ QDs	Physical blending	Water (immersion)	PL	60%	88% (86%)	1 month	142
$CsPbBr_3$ QDs–poly(styrene-ethylene-butylene-styrene) films	Physical blending	Water (immersion)	PL	—	—	122 days	143
V18–$MAPbBr_3$ NCs	Thermal polymerization	Water (immersion)	PL	85%	—	120 min	133
V18-*co*-MMA-$MAPbBr_3$ NCs	Thermal polymerization	Water (immersion)	PL	—	—	90 days	133
Crosslinked PETA-G/$FA_{0.92}MA_{0.08}PbI_3$ films	Spin-coating and thermal polymerization	Water (immersion)	Photograph evolution	—	—	420 s	144
$CsPbBr_3$/polypyrrole	Visible light polymerization	Water (immersion)	PXRD TEM	—	—	30 days	145
$CsPbBr_3$/polyaniline	Visible light polymerization	Water (immersion)	PL PXRD TEM	~93%	—	4 weeks	146

[a] NOA61: Norland Optical Adhesives 61; Ergo: Ergo® optical adhesive 8500; PMSR: phenyl methyl silicon resin; SSDC: Silicone Sealant Dow Corning® 937; PMA: poly(isobutylene-alt-maleic anhydride)-*graft*-dodecyl; $R_{pol/area}$: the number of monomers of polymer per NP area [nm^2]; Hyflo: Hyflon AD 60; DFTHS: dodecafluoroheptylpropyl-trihydroxysilane; V18: 4-vinylbenzyl-dimethyloctadecylammonium chloride.

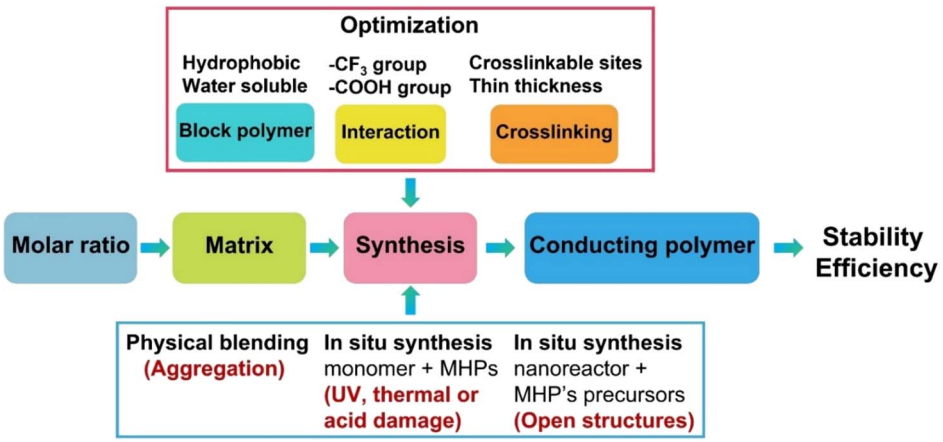

Fig. 5 Scheme of suggested strategies for the synthesis of polymer–MHPs composites.

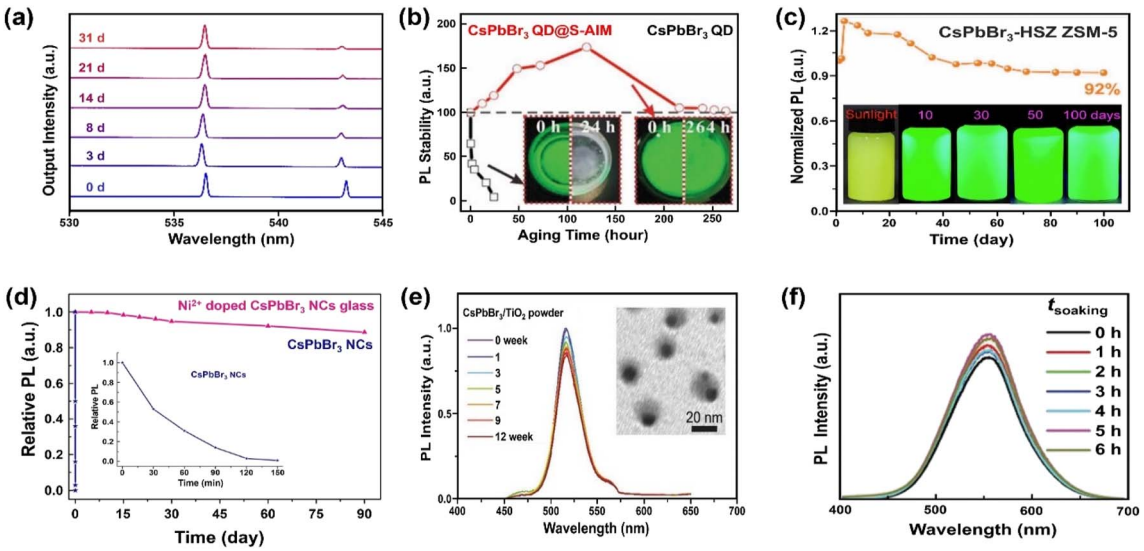

Fig. 6 Stabilizing MHPs by using inorganic materials. (a) Time-dependent normalized lasing spectra of the ALD Al_2O_3 coated $CsPbBr_3$ nanoplate after being immersed in water for 1 month. Adapted from ref. 158. Copyright 2020 American Chemical Society. (b) PL intensity evolution over $CsPbBr_3$ QDs and $CsPbBr_3$ QDs@superhydrophobic aerogel inorganic matrix (S-AIM) completely immersed in water with time. Adapted from ref. 163. Copyright 2020 John Wiley and Sons. (c) PL stability of $CsPbBr_3$-HSZ ZSM-5-700 composites when exposed in water and luminescent photographs of $CsPbBr_3$-HSZ ZSM-5-700 composite immersed in water for various time (5 mg mL^{-1}). Adapted from ref. 175. Copyright 2022 Elsevier. (d) The change in relative PL of Ni^{2+} doped $CsPbBr_3$ NCs glass and $CsPbBr_3$ NCs in water (inset: enlarged the change of PL with $CsPbBr_3$ NCs in water). Adapted from ref. 177. Copyright 2019 Elsevier. (e) The relative PL intensity of $CsPbBr_3/TiO_2$ NCs after immersing in Milli-Q water (0–12 weeks), inset shows a TEM image of $CsPbBr_3/TiO_2$ NCs after immersing in Milli-Q water for 12 weeks. Adapted from ref. 181. Copyright 2017 John Wiley and Sons. (f) Normalized PL spectra of $Cs_2Sn_{0.89}Te_{0.11}Cl_6$ *versus* different soaking time. Adapted from ref. 180. Copyright 2020 John Wiley and Sons.

from rough surface,[196] and the hydrophobic functional groups from the AGs.[163]

However, the open shell after impregnation is still a threat to long-term stability. Thus, a second coating is normally needed. For this purpose, ALD grown compact AlO_x,[168] polymers[169,170] and biomedical phospholipids[171,172] have been reported. The $mSiO_2$–$CsPbBr_3$@AlO_x obtained with 100 ALD cycles keeps up to 95% of PL intensity after 8 h in water dispersion under stirring, and the stability extends to 90 days under static conditions.[168] He *et al.* embedded Mn-doped $CsPbCl_3$ QDs into SiO_2/Al_2O_3 monolith through a facile sol–gel process, followed by a physical grinding. The obtained Mn-doped $CsPbCl_3$ QDs-SiO_2/Al_2O_3 monolith sample maintained around 92% of the initial PL intensity after 7 days under accelerated aging condition (85 °C and 85% RH).[173] For polymers, this strategy can trigger the formation of micro/nano structured SiO_2 surface, which is one essential feature needed for super-hydrophobicity.[197,198] The coating of biomedical phospholipid can also further improve the stability over SiO_2 coated MHPs and broaden their applications in bioimaging and biosensing.[171,172]

Another issue is the aggregation during the synthesis, which may cause quenching and instability.[124,199] In conjunction with

polymer-type coatings, most of the studies focus on multiple MHP NCs. However, the synthesis of monodisperse MHP NCs at atomic-level is more desirable in LEDs, bio- or catalysis-related fields. Through a fast hydrolysis of highly reactive silica precursor (for example, tetramethoxysilane, TMOS) with a small amount of water, the MHP NCs or QDs can be wrapped by silica at the interface of water/nonpolar solvent *via* a simple sol–gel method to synthesize monodisperse $CsPbX_3/SiO_2$ nanoparticles.[159] The $CsPbBr_3/SiO_2$ Janus NCs suspension showed bright PL and remained 80% of the PL intensity after placing in water 7 days.[159] This method can be extended to other oxides, such as Ta_2O_5, ZrO_2.[160] However, the Janus structure means that part of the surfaces of MHPs are exposed to the environment simultaneously and would suffer from degradation. Subsequent work by Zhang's group has achieved monodisperse $CsPbBr_3@SiO_2$ core–shell nanoparticles with the aid of ammonia *via* a modified supersaturated recrystallization method. They also found that ammonia is not mandatory for hydrolysis, but influences the morphology, size of the products and the formation rates of SiO_2. Under a harsh condition (ultrasound irradiation in water for 40 min), $CsPbBr_3@SiO_2$ core–shell nanoparticles still exhibited bright emission.[161]

SiO_2 is usually synthesized by the hydrolysis of Si precursor *via* a sol–gel method. Note that the choice of precursor and synthetic methods will also impact the water stability of MHP–SiO_2 composites. Owing to the fast hydrolysis rate of TMOS, it is widely used in synthesis of highly stable MHP–SiO_2 composites.[159,161] However, it is reported that the MHP–SiO_2 composites synthesized *via* a modified ligand-assisted reprecipitation (LARP) method showed a lower stability in water, probably caused by the amorphous and porous structure.[164] Generally, tetraethoxysilane (TEOS) has been regarded as an inefficient precursor to envelop MHP NCs owing to its slower hydrolysis rate, which would form separate MHP NCs or big aggregates. However, monodisperse $CsPbBr_3@SiO_2$ NCs has been reported by using TEOS *via* one-pot hot-injection strategy.[165] By introducing the hydrophobic and multibranched trioctylphosphine oxide (TOPO) as ligands, the TOPO would anchor on the surface of NCs, and effectively tune the hydrolysis rate of TEOS and surface property of NCs resulting in the formation of core@shell NCs at a nanoscale-particle level. The $CsPbBr_3@SiO_2$ NCs retained more than 70% of their initial fluorescence intensity within 8 days immersion in hexane–water (1/1.5, v/v) mixture. Accordingly, based on these results, we may conclude that the quality of SiO_2 and hence its barrier properties strongly depend on the synthetic routes applied.

Besides the choice of suitable precursors, the interaction of SiO_2 and MHPs would also influence the final water stability. It is found that coatings produced from phenyltriethoxysilane (phTEOS) could not envelope the MHP NCs because of the weak adsorption of intermediate silsesquioxanes over MHPs.[200] Only combining TMOS with phTEOS (especially equimolar amount), the MHPs can be covered by 3D silica grafting with hydrophobic phenyl group, showing an improved water-resistance (at least for 24 hours).[164] The interaction can be strengthened by the addition of interfacial ligands (such as PVP[166]) or the introduction of bonding interactions.[167] For example, Li *et al.* have introduced a Pb–S bonding by directly using (3-mercaptopropyl) trimethoxysilane ($C_6H_{15}O_3Si$-SH, MPTMS) as SiO_2 precursor.[167] The strong bonding makes the perovskite@silica nanodots stable in water for over six weeks.

Zeolites represent a large family of inorganic porous crystalline materials, in which the anions of $[AlO_4]^{5-}$ and $[SiO_4]^{4-}$ tetrahedra are linked with oxo-bridges forming networks of 3D cages or channels.[201] The pore structure makes them vastly used in catalysis, separation, gas adsorption and ion-exchange.[202,203] Cation exchange property of zeolite can activate the introduction of A site ions from MHPs, and the $CsPbBr_3$ QDs can grow into the zeolite structure *via in situ* crystallization. Such composites exhibit excellent photostability[204] and water resistance.[174] Contrary to the commonly recognized $CsPbBr_3$ QDs, new species of $[Na_4Cs_6PbBr_4]^{8+}$ QDs have been confirmed in the zeolite's super cage, in which the tetrahedral $PbBr_4^{2-}$ ions are surrounded by Na^+ and Cs^+ ions. A recent study has shown that the high water-resistance (for 100 days) of $CsPbBr_3$ QDs-HSZ ZSM-5 (Fig. 6c) is attributed to the interconnected micro–mesoporous network in hierarchically structured zeolite (HSZ). The micropores act as a shielding wall to isolate MHPs from the external environment and mesopores promote the diffusivity of precursors towards the successful space-confinement of $CsPbX_3$ (X = Cl and Br) QDs.[175]

As an alternative, inorganic glass matrices (silicate, soda-lime, lead-oxide *etc.*) have been proven as another effective way to stabilize MHPs. The glass matrixes feature excellent mechanical, thermal and chemical stability. Up to now, mostly $CsPbX_3$ NCs have been successfully incorporated into glass matrices, demonstrating dramatic enhancement of water stability, up to 90 days (Fig. 6d).[176,177] This solution needs high processing temperature, which would unavoidable to engender the volatilization of halides precursor (*e.g.*, CsBr and $PbBr_2$).[205] It has been reported that embedding $CsPbBr_3$ QDs into TeO_2-based inorganic glass can lower the temperature (from 1100 °C to 630 °C). However, the water stability decreases to 120 hours correspondingly.[178] However, the glass matrix is only studied in all-inorganic MHPs because of their higher thermal stability and structure integrity during the formation process of glass.

Although the encapsulation with AlO_x, SiO_2, zeolites and glassy materials can solve the instability issue of MHPs, similar to the non-conductive organic polymers or ligands, these insulating materials restrain charge extraction across the coating shell and thus greatly disable applications in catalysis. Therefore, instead, application of semiconducting inorganic coating materials such as SnO_2 and TiO_2 can be a more viable option. Apart from enabled carrier transport, another benefit of semiconducting coatings is a possibility to have electron–hole rectification across the interfacial junctions (depending on the band structures of the core and shell materials), which can eventually inhibit/delay recombination.[206] Stable $CsPbBr_3/TiO_2$ core/shell NCs have been reported by calcination of $CsPbBr_3$ NCs and titanium butoxide at 300 °C for 2 h.[181] The tight TiO_2 shell over $CsPbBr_3$ core ensures the stability of PL peak position and intensity ($\approx$80%) for over three months (Fig. 6e). To obtain a robust protecting layer, crystalline TiO_2 is favored over an amorphous phase.[207] However, the poor thermal stability of

MHPs (mostly blow 300 °C for hybrid ones[208]) limits the thermal budgets of processes. In contrast to the instability of amorphous TiO_2 shell, amorphous SnO_2 obtained by hydrothermal route was found to be able to stabilize $Cs_2Sn_{1-x}Te_xCl_6$ ($x = 0.11$)[180] and $Cs_2Pt_xSn_{1-x}Cl_6$ ($0 \leq x \leq 1$)[209] solid solutions in water (Fig. 6f). Thus, it appears that not only the choice of the inorganic materials coating but also the chemistry plays a role in water stability of the core (Table 3). However, it is worth noting that both TiO_2 and SnO_2 absorb only in the UV region, which only accounts for less than 4% in solar spectrum.

2.1.4 MOFs. Metal–organic frameworks (MOFs) have been investigated as photocatalysts for HER in addition to other energy conversion applications.[210] Compared with porous zeolites, MOFs possess highly tunable pore sizes and tailorable chemistry beyond large specific surface areas.[211] The hydrophobic wall inside MOF provides excellent water protection and the cavities can host perovskites to prepare nanoparticles@MOF composites *via in situ* growth or post-encapsulation.[212] Zhang *et al.* encapsulated the $CH_3NH_3PbBr_3$ QDs in hydrophobic MOF-5 *via* a two-step synthesis procedure. The obtained $CH_3NH_3PbBr_3$@MOF-5 composites showed stable green emission after 30 days of immersion in water (Fig. 7a).[213] However, there are some drawbacks over these methods because some MHPs would be attached on the surface of MOFs instead of the cavities.[213,214] The exposed MHPs pose a threat to the stability of MHP@MOF composites, and it is important to confine the MHPs within the cavities completely (Fig. 7b). For this point, Mollick *et al.* synthesized water-stable MOF (namely, zeolitic imidazolate framework, ZIF-8) capped $MAPbBr_3$ by washing the product thoroughly with DMF to remove surface perovskites.[215] After dipping in water for 90 days, the composite retained over 70% intensity of luminescence (Fig. 7c).

Apart from the removal of surface MHPs, the stability and the pore size (cavity diameter and opening aperture size) of MOF matrix also dominate the water stability of MHP@MOF. The MOF should be stable during the synthesis of composites, and the pore size should be well-tailored, which can accommodate monodispersed MHP nanoparticles in the cage, but also suppress the MHP leaching through the opening apertures. For instance, to confine the monodispersed $CsPbBr_3$ nanocrystals (4–5 nm) into MOF, mesopores (pore size >4 nm) instead of common micropores (*e.g.*, ZIF-8, pore size <4 nm)[216] are desirable, since the MHP NCs can grow freely inside the cage and would not damage the porous structure of MOFs. To this end, Yu and coauthors utilized the high-valent metal-based MOF (PCN-333(Fe)) as host and constructed a $CsPbBr_3$@PCN-333(Fe) composite material, working as a stable photocathode in Li–O_2 battery for at least 200 hours.[217] In addition, the long-channel of MOF can also serve as a template for the growth of MHP nanowires. Xia *et al.* reported that the $CsPbI_3$ nanowires can be grown and encapsulated into Zr-based MOF (PCN-222). The $CsPbI_3$@PCN-222 maintained structure integrity (Fig. 7d) and morphology after water immersion for 72 h due to the excellent protection of the MOF walls.[218]

Another breakthrough over MOF has been reported by Hou and coworkers. They have successfully prepared $(CsPbI_3)_{0.25}$-$(a_gZIF\text{-}62)_{0.75}$ composites at 350 °C by liquid-phase sintering (ZIF-62, $\{Zn[(Im)_{1.95}(bIm)_{0.05}]\}$; Im, imidazolate; bIm, benzimidazolate). The composites extended water stability up to over 10 000 hours.[219] Compared to the silica-based glasses mentioned earlier, the ZIF glasses can be prepared at a lower temperature[220] because of the metal–imidazolate–metal linkages and large voids.[221]

2.1.5 Phase engineering. Phase engineering provides an efficient way to tailor the nanomaterials surface characteristics and physicochemical properties.[222] This strategy has been employed for transition metal dichalcogenides to construct new nanostructures having improved charge injection[223] and catalytic activity.[224] Inspired by this, constructing new phases over MHPs would bring enhanced stability and carrier extraction efficiency. Unlike hybrid MHPs forming a single compound, the nonstoichiometric precursor of all-inorganic MHPs will favor the formation of different compounds (for example, Cs_4PbBr_6, $CsPb_2Br_5$, and $CsPbBr_3$) according to the phase diagram.[225] Conventional ligands (OA and OAm) induce fast dissolution of $PbBr_2$ and the resulting solution contains $[PbBr_4]^{2-}$, $[PbBr_3]^-$, $[PbBr_6]^{4-}$ intermediate species,[226] leading to mixtures of various phases (Fig. 8a).[227,228] The successful synthesis of pure single phase is quite challenging[227,229–231] (Fig. 8a, highlight in red) because many factors would influence the final products, including the stoichiometric ratio, ligand, temperature, and solvent used.

Dual phases such as $CsPbBr_3$–$CsPb_2Br_5$ NCs[232] and $CsPbBr_3$/Cs_4PbBr_6 NCs[233] seem to show enhanced stability. With excess $PbBr_2$, $CsPbBr_3$/$CsPb_2Br_5$ core–shell NCs have been synthesized *via* a modified non-stoichiometric solution-phase method.[234] Layered 2D $CsPb_2Br_5$ nanosheets are coated on the surface of $CsPbBr_3$ nanocubes. The $CsPbBr_3$/$CsPb_2Br_5$ core–shell NCs remained luminous after ultrasonication in water for 2 h. The elevated stability originates from the unique sandwiched structure of 2D $CsPb_2Br_5$ in which the Cs^+ ions are inserted into the compact-bound inorganic $(Pb_2Br_5)^-$ layers *via* strong electrostatic interactions.[235,236] Further improvement of water stability was realized with Sb^{3+}-doped dual-phase $CsPb_2Br_5$/$CsPbBr_3$ NCs (preserving 80% of the original PL value up to 30 days, Fig. 8b).[237] This is because the replacement of Pb^{2+} (1.19 Å) ions with smaller Sb^{3+} ions (0.92 Å) leads to increased lattice energy.[238] Meanwhile, rapid hydrolysis of Sb^{3+} ions in water may also play a role.[239,240] The presence of hydrophobic antinomy oxychloride in Sb-doped MHPs is also considered to be the reason for improved water stability.[238,241,242]

2.1.6 Water-assisted engineering. As mentioned, MHP structures exhibit some tolerance to water for short time periods. It has been reported that moisture has a vital role in the quality of perovskite film, which is evidenced by the significant improvement in PL and photovoltaic performance after annealing under 65% RH at 90 °C for 30 min.[243] To understand how moisture influences the MHPs, Eperon *et al.* proposed a 'self-healing' process, in which solvated and mobile MA^+ ions in water can 'heal' the perovskite structure.[58] The easy mobility of MA^+ ions or Cs^+ ions in water inspires to prepare water-stable MHPs *via* CsX-stripping strategy. For example, CsX-rich 0D Cs_4PbX_6 NCs can be stripped into 3D $CsPbX_3$ NCs at the water/hexane interface and the obtained $CsPbX_3$ NCs keep stable after

Table 3 Inorganic materials used for synthesis of water-stable MHPs

Water-stable MHPs		Stability					
Materials	Methods	Medium	Characterizations	Retained PL intensity	PLQY before (after)	Observed durability	Ref.
$CsPbX_3$ QDs/AlO_x films	ALD	Water (immersion)	PL	100%	—	>1 h	157
Al_2O_3-coated $CsPbBr_3$ nanoplate	ALD	Water (immersion)	Lasing spectra	—	—	31 days	158
$CsPbBr_3/SiO_2$	Water-triggered transformation and sol–gel method	Hexane/water (floating)	PL	80%	80% (—)	7 days	159
$CsPbBr_3/ZrO_2$-10	Water-triggered transformation and sol–gel method	Hexane/water (floating)	PL	80%	90% (—)	8 days	160
$CsPbBr_3$@SiO_2 NPs	Modified supersaturated recrystallization	Water (ultrasonication, suspension)	PL	—	—	40 min	161
$CsPbBr_3$ QDs/mesoporous silica AGs	Physical blending	Water (immersion)	PL	50%	—	14 days	162
Green-S-AIM/$CsPbBr_3$ QDs	Postadsorption	Water (immersion)	PL	100%	75.6% (50.5%)	11 days	163
Green-S-AIM/$CsPbBr_3$ QDs	Postadsorption	Hexane/water (floating)	PL	—	75.6% (77.6%)	4.5 months	163
phTEOS-TMOS@$CsPbBr_3$ NCs	Hydrolysis-condensation	Water (immersion)	PL PXRD FTIR	—	—	24 h	164
$CsPbBr_3$ QDs@SiO_2	Nonpolar solvent	Hexane/water (floating)	PL	70%	~87% (—)	8 days	165
PVP–$CsPbBr_3$ QD@SiO_2-octadecyl trimethoxysilane-lecithin core–shell nanoparticles	Physical blending, hydrolysis-condensation and self-assembly	Water (immersion)	PL	98%	41.6% (—)	10 days	166
$CsPbBr_3$ QDs-Pb-S-SiO_2-SH nanodots	Hydrolysis-condensation	Water (suspension)	PL	50%	78% (—)	20 days	167
$CsPbBr_3$ QDs-Pb-S-SiO_2-SH nanodots	Hydrolysis-condensation	Water (suspension)	PL	—	—	6 weeks	167
Mesoporous SiO_2–$CsPbBr_3$@AlO_x	Modified template-assisted formation and ALD	Water (suspension)	PL	95%	—	8 h	168
Mesoporous SiO_2–$CsPbBr_3$@AlO_x	Modified template-assisted formation and ALD	Water (suspension)	PL	20%	—	90 days	168
$MAPbBr_3$@SiO_2/PVDF nanoparticles	Impregnation and physical blending	Water (floating)	PL	—	85.5% (—)	1 month	169
$MAPbBr_3$@SiO_2/PVDF films	Impregnation and C	Water (immersion)	PL	83%	85.5% (—)	20 min	169
$MAPbBr_3$@SiO_2/PVDF films	Impregnation and physical blending	Water (immersion)	PL	55%	85.5% (—)	2 h	169
$CsPbI_3$@polystyrene@SiO_2	Confined condensation	Water (boiling)	PL	97.8%	86% (—)	48 h	170

Table 3 (*Contd.*)

Water-stable MHPs		Stability					
Materials	Methods	Medium	Characterizations	Retained PL intensity	PLQY before (after)	Observed durability	Ref.
$CsPbBr_3/SiO_2$/PEGylated phospholipid	Hydrolysis-condensation and physical blending	Water (suspension)	PL	80%	—	2 weeks	171 and 172
Mn-doped $CsPbCl_3$ QDs-SiO_2/Al_2O_3 monolith	One-pot synthesis	85 °C and 85% RH	PL	~92%	—	7 days	173
$[Na_4Cs_6PbBr_4]^{8+}$-zeolite	Ion-exchange and *in situ* growth	Water (immersion)	PL PXRD XPS	100%	35% (—)	40 days	174
$CsPbBr_3$ QDs-HSZ ZSM-5	Grinding-calcination	Water (immersion)	PL	92%	62% (—)	100 days	175
$CsPbBr_{1.2}/I_{1.8}$ NCs@P-Si-Zn glass	Melt-quenching and subsequent heat-treatment	Water (immersion)	PL	~90%	—	40 days	176
Ni^{2+}-doped $CsPbBr_3$ NCs@B-Si-Zn glass	Melt-quenching	Water (immersion)	PL	88.2%	84.3% (—)	90 days	177
$CsPbBr_3$ QDs@TeO_2-based glass	*In situ* nanocrystallization	Water (immersion)	PL	~90%	70% (—)	120 h	178
$CsPbBr_3$ QDs@TeO_2-based glass	*In situ* nanocrystallization	Water (immersion)	PL	~60%	70% (—)	45 days	178
$CsPbBr_3$@ZnO nanoparticles	Physical blending	Water (ultrasonication)	PL	—	—	30 min	179
$CsPbBr_3$@$NaYF_4$ nanoparticles	Physical blending	Water (ultrasonication)	PL	—	—	30 min	179
$Cs_2Sn_{0.89}Te_{0.11}Cl_6$	Hydrothermal method	Water (immersion)	PL PXRD FTIR XPS	100%	95.42% (—)	360 min	180
$CsPbBr_3/TiO_x$	Hydrolysis-drying	Water (immersion)	PL	—	—	1 week	181
$CsPbBr_3/TiO_2$ core/shell NCs	Hydrolysis-calcination	Water (immersion)	PL TEM PXRD	~85%	—	3 months	181

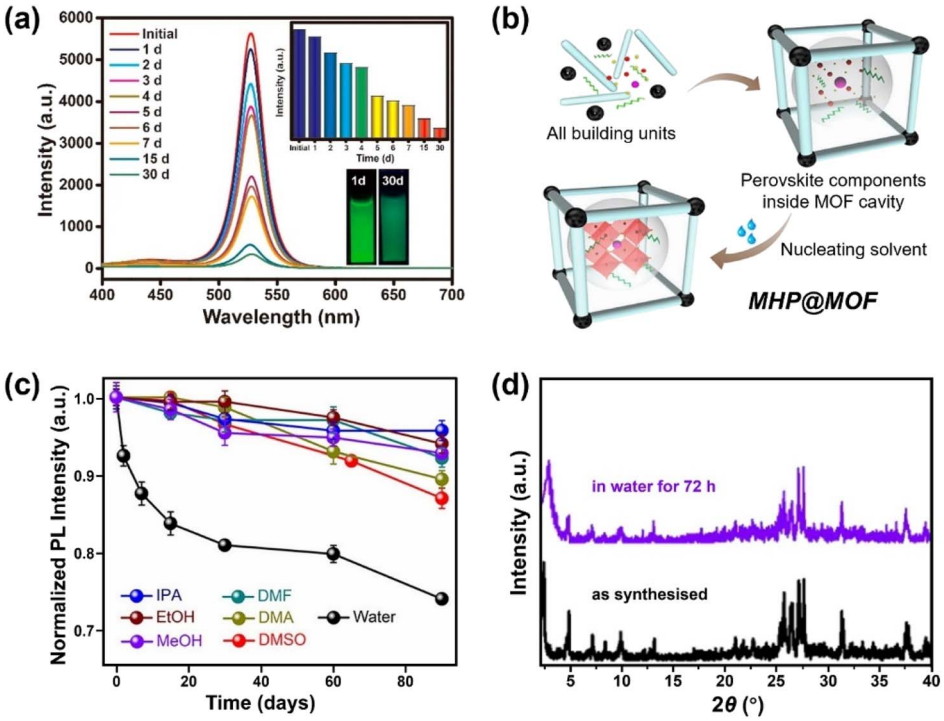

Fig. 7 MHPs encapsulated by MOF. (a) Time-dependent PL spectra of $CH_3NH_3PbBr_3$@MOF-5 composites in water for different days (inset: the evolution of PL intensity and the images of $CH_3NH_3PbBr_3$@MOF-5 composites under 365 nm light after 1 and 30 days). Reproduced with permission from ref. 213. Copyright 2018 American Chemical Society. (b) Scheme for preparing MHP@MOF composites and (c) normalized PL intensity as a function of time in different polar solvents over a period of 90 days. Adapted from ref. 215. Copyright 2019 American Chemical Society. (d) XRD patterns of $CsPbI_3$@PCN-222(20%) before and after immersion in water for 72 h. Adapted from ref. 218. Copyright 2022 John Wiley and Sons.

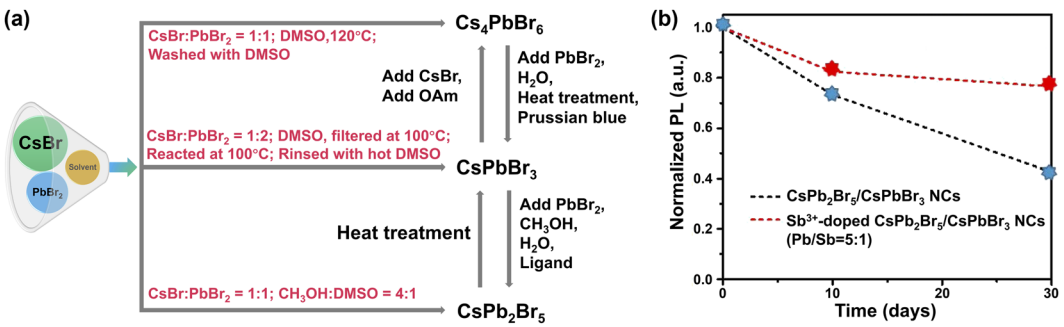

Fig. 8 Phase engineering. (a) Schematic diagram illustrating the synthesis of pure $Cs_XPb_YBr_Z$-based MHPs and their potential transformations. (b) PL intensity of $CsPbBr_3/CsPb_2Br_5$ NCs and Sb^{3+}-doped dual phase $CsPbBr_3/CsPb_2Br_5$ NCs (Pb/Sb = 5 : 1) as a function of time. Adapted from ref. 237. Copyright 2021 Elsevier.

36 h storage.[244] This strategy was further extended to exfoliate 0D Cs_4PbX_6 NCs into water-stable quasi-2D $CsPbBr_3$ nanosheets,[245] 1D $CsPbBr_3$ nanowires, 2D $CsPbBr_3$ nanoplatelets, and 3D $CsPbBr_3$ nanocubes.[246]

The reasons for the enhanced stability are manifold. As depicted in Fig. 9a, one is the dissolution of the defective surface and thus the formation of near to ideal stoichiometry ($CsPbBr_3$) having high stability.[247,248] Benefiting from improved crystal quality of MHP NCs and the immiscibility of hexane with water, further dissolution of $CsPbBr_3$ NCs would not happen temporarily. Another explanation is the concurrent passivation and the formation of halide-rich surface upon CsX-stripping.[249] The origin of this passivation results from the dissolution of surface layers of MHP NCs during the CsX-stripping process and subsequently the formation of non-stoichiometric MHP surface (Fig. 9b).[250,251] For example, with Cs_4PbBr_6 NCs as starting materials, the following water treatment engenders a phase transformation into $CsPbBr_3$, accompanied by a passivation effect from the CsBr salt in water. The resultant $CsPbBr_3$ NCs display ultra-stability (over 200 days with ~20% decrease in the initial PL value, Fig. 9d).[250] A third potential mechanism is based on the attached isomorphic hydroxyl (OH)

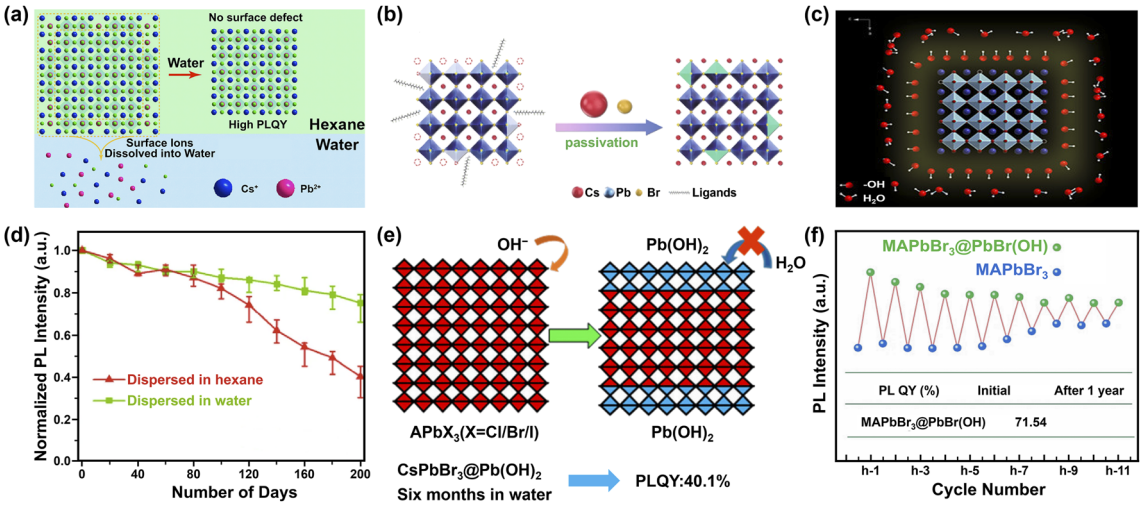

Fig. 9 Water-assisted engineering for preparing water-stable MHPs. Three possible mechanisms (a–c) for the synthesis of water-stable MHPs with water-assisted engineering strategy: (a) illustration of forming $CsPbX_3$ NCs in hexane with perfect unit cell after water-treatment. Adapted from ref. 247. Copyright 2018 American Chemical Society. (b) Schematic diagrams of $CsPbBr_3$ NCs passivated by CsBr. Reproduced with permission from ref. 250. (c) Illustration of $CsPbBr_3$ NCs stabilized by hydroxyl (OH) ligands. Reproduced from ref. 88. (d) Normalized PL intensity's evolution of $CsPbBr_3$ NCs dispersed in water and hexane respectively. Adapted from ref. 250. (e) Formation mechanism of $Pb(OH)_2$ by Lewis base vapor diffusion (LBVD) method. Adapted from ref. 259. Copyright 2018 American Chemical Society. (f) The variant PL intensity of $MAPbBr_3$@PbBr(OH) and $MAPbBr_3$ during cycling. Adapted from ref. 261.

ligands over $CsPbBr_3$ nanocrystals that are assumed to prevent MHP NCs from further water attack (Fig. 9c).[88] The formation of hydroxyl might have originated from the self-ionization of water. It is reported that polar solvent (for example, isopropanol, C_3H_7OH) will ionize itself to produce $C_3H_7O^-$ and $C_3H_7OH_2^+$ and replace OA^- and OAm^+ respectively, acting as shorter and more reactive ligands and inducing the oriented growth of MHP NCs.[252] Similar ionization is expected in the case of water, which triggers the formation of OH ligands on MHP NCs.[253] Additionally, the hydroxyl groups might provide a passivation effect by forming hydrogen bonding interaction with halide ions in MHPs.[254] Besides these possibilities, the formation of atomically thin quasi-2D $CsPbBr_3$ nanosheets (NSs) also favors the stability,[245] because the (quasi-)2D structures features improved stability[255] and suppressed ion migration[256] than their 3D counterparts.

Efforts have been devoted to decoding the underlying mechanism with density-functional theory (DFT) calculations. Recent studies indicate that Cs-rich precursor favors the formation of CsBr-terminated surface, whereas low Cs concentration results in $PbBr_2$ terminations. Compared with $PbBr_2$-terminated surface, the former case is more stable even after the adsorption of water molecules according to the DFT results.[257] Yoo *et al.* proposed that a ligand transition from anionic ligands to cationic ligands in metal halide medium also contributes the improved water stability.[258]

In situ grown $Pb(OH)_2$ *via* a Lewis base vapor diffusion (LBVD) method has been proposed as another strategy to stabilize the MHPs (Fig. 9e).[259] When excess methylamine is diffused into the solution of MHPs, a basic solution (pH > 12) is formed. Then highly nucleophilic OH^- ions react with the peripherical layer of $[PbX_6]^{4-}$ on MHPs, forming a dense $Pb(OH)_2$ layer. Notably, the as-obtained $Pb(OH)_2$-coated perovskites maintained structural stability in water for more than 6 months and retained the fluorescence property in water even after grinding or sonication. The $Pb(OH)_2$-coated $MAPbX_3$ perovskites can be also obtained *via* organic cation exchange between formamidinium (FA^+) and MA^+ in water, which can further extend the stability up to one year.[260] Instead of the time-consuming LBVD method, to form surface hydroxides may be obtained by simply adjusting the pH of metal halide precursor solution with ammonium hydroxide.[261,262] Such $MAPbBr_3$@PbBr(OH) retained 89.9% of the initial PL value (*i.e.*, 64.28%) after being immersed in water for 1 year (Fig. 9f). The PbBr(OH) layer can be also extended to all-inorganic MHPs. For example, by modulating the water content, water-stable $CsPbBr_3/CsPb_2Br_5$@PbBr(OH) and $CsPbBr_3$@PbBr(OH) nano/micro-spheres have been obtained respectively, in which $CsPbBr_3/CsPb_2Br_5$@PbBr(OH) showed excellent water stability and maintained 91% of initial PL intensity after 18 months of storage in water.[263] Dong *et al.* also found that rod-like $CsPb_2Br_5$-embedded Pb(OH)Br obtained 92.2% of initial PL intensity after soaking in water for 165 days, indicating a good stability.[264] PbBrF matrix also shows good protecting ability in $CsPbBr_3$/PbBrF composites having no decrease of PLQY after 30 days in water.[265] DFT calculations indicated that the improved stability originates from the increased decomposition enthalpy after introducing insoluble PbBr(OH) compared with that of bare $MAPbBr_3$ (ref. 261 and 263) or the positive energy cost for water entering the lattice of PbBr(OH).[266]

Even though water-assisted engineering strategy can dramatically improve MHPs stability in water, it should be mentioned that no photocatalytic applications over this class of water-stable MHPs have been reported yet.

2.2 Common-ion effect

It is well-known that a salt can be precipitated by adding other soluble salts having common ions to the solution. Inspired by this, Nam's group have proposed the idea of common-ion effect to prepare water-stable MHPs in aqueous solution.[28] Although the MHPs are stabilized, it is a difficult-to-implement strategy in the practice due to the highly corrosive nature of the solution (pH < −0.5 and $[I^-]$ > 2.5 mol L^{-1}). Clearly, a more practical medium is needed. Later, Geng *et al.* found that $CH_3NH_3PbX_3$ (X = Br or Cl/Br) nanocrystals could be synthesized in aqueous solution when the pH value was in the range of 0–5.[267] In this aqueous solution, the $[PbX_6]^{4-}$ ions would adsorb on NCs, facilitating the formation of halide-rich surface of NCs, thus preventing the dissolution of MHP NCs in water. However, they would decompose in neutral solution.

To realize the water stability of MHPs, our group explored to employ the bismuth halide perovskites as photocatalysts owing to their better stability in solar cells and photocatalysis.[268–270] We found that the tri(dimethylammonium) hexaiodobismuthate (DA_3BiI_6) could be stabilized in aqueous solution using dimethylammonium iodide (DAI) without addition of acids.[271] We noted that a stepwise transformation of BiI_3 → $[BiI_4]^-$ → $[BiI_6]^{3-}$ as the increase of DAI concentration and only $[BiI_6]^{3-}$ ions existed when the concentration of DAI was higher than 0.15 M (Fig. 10a and b). The structural integrity of DA_3BiI_6 could be preserved for more than two weeks (Fig. 10c and d). Similarly, a series of 2D MHPs, including $C_6H_5CH_2NH_3PbI_4$, $C_6H_5(CH_2)_2NH_3PbI_4$ and $C_6H_5(CH_2)_3NH_3Pb_2I_7$ have been stabilized in iodide salt aqueous solutions.[272]

2.3 Intrinsic water stability

Besides the strategies developed based on surface engineering and common-ion effect discussed above, exploring intrinsically water-stable MHPs are potentially advantageous because they can bypass the obstacles of water instability in aqueous media.

A few 3D MHPs have exhibited an intrinsic stability in water. As far as we know, the first reported intrinsically water-stable MHPs were hydroxyl ammonium lead iodo chloride ($OHNH_3PbI_2Cl$) and hydroxyl ammonium lead chloride ($OHNH_3PbCl_3$).[273] After stirring in deionized water for 1 h, no leaching of Pb^{2+} was detected. In addition, no color change of the solids was observed after a 45 days immersion in water, suggesting outstanding water-stability. It is speculated that strong hydrogen bonding interactions among MHPs contribute to the water stability. However, it is worth noting that their crystal structures are still under dabate.[274,275] Also, $C_6H_4NH_2CuBr_2I$ with ABX_3 structure has exhibited no structure change after water immersion for 4 h.[276,277] Currently, another widely studied water-stable MHPs are dimethylammonium tin halide perovskites,[278,279] which feature no decomposition after 20 h in deionized water (see Fig. 11a). Based on DFT calculations (Fig. 11b), the intrinsic water-stability originates from higher

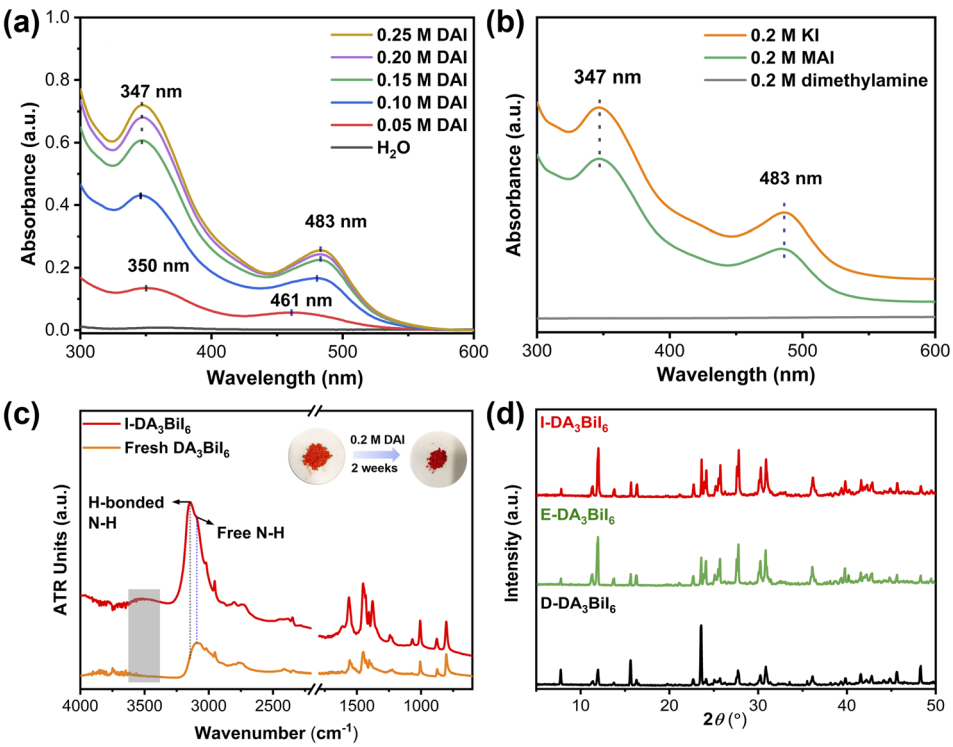

Fig. 10 Common-ion effect. (a) UV-vis absorption spectra of DAI aqueous solutions after immersing DA_3BiI_6 for 1 day. (b) UV-vis absorption spectra of 0.2 M aqueous dimethylamine, KI, and MAI solutions after immersing DA_3BiI_6 for 5 min. (c) ATR-FTIR spectra and color change of DA_3BiI_6 and immersed-DA_3BiI_6 powder. (d) XRD patterns of DA_3BiI_6 after immersion in water, ethanol and DA_3BiI_6 synthesized from DAI. Reproduced from ref. 271.

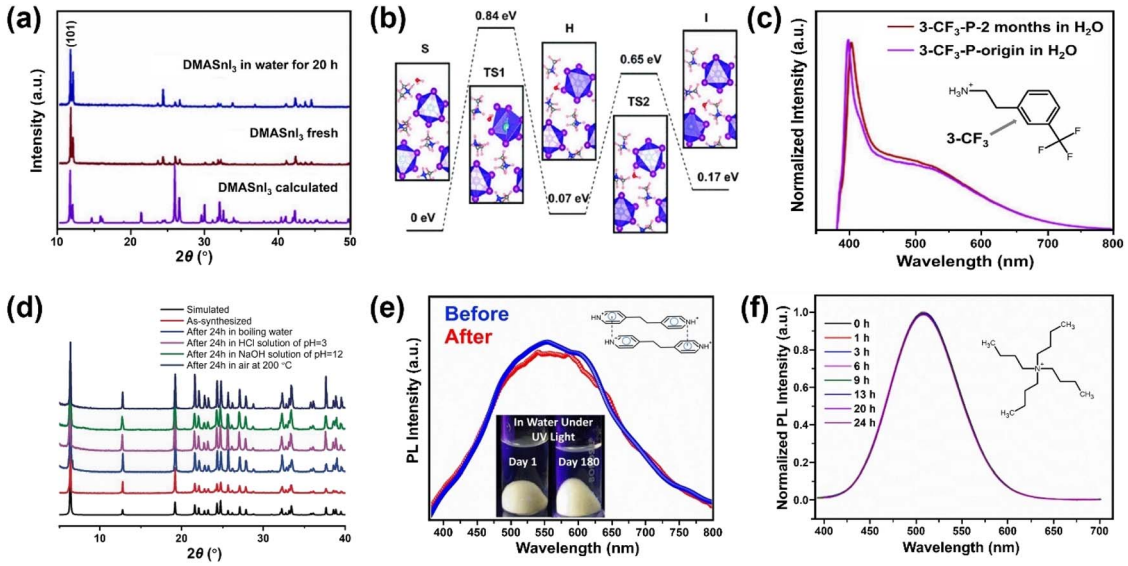

Fig. 11 Intrinsically water-stable MHPs. (a) The powder XRD (PXRD) patterns of $DMASnI_3$ before and after water treatment. Adapted from ref. 279. Copyright 2020 John Wiley and Sons. (b) Relative energy profile for water infiltration into (101) surface of $DMASnI_3$ crystal. Adapted from ref. 279. Copyright 2020 John Wiley and Sons. (c) PL spectra of 3-CF_3-MHP before and after being kept in water for 2 months. Adapted from ref. 285. Copyright 2022 American Chemical Society. (d) PXRD patterns of $[Pb_2Cl_2]^{2+}$ $[^-O_2C(CH)_2CO_2^-]$ before and after chemical treatment for 24 h. Adapted from ref. 288. Copyright 2017 John Wiley and Sons. (e) PL spectra of fresh and immersed (4,4′-EDP)Pb_2Br_6 for 180 days. Adapted from ref. 294. Copyright 2021 John Wiley and Sons. (f) Normalized PL spectra evolution of $(C_4H_9)_4NCuCl_2$ after water immersion for different periods. Adapted from ref. 296. Copyright 2021 American Chemical Society.

water surface adsorption energy, higher water osmotic energy barrier, and smaller intralayer spacing inside $DMASnI_3$ structure compared with the Pb-based counterpart.[279]

In contrast to 3D MHPs, low-dimensional (2D, 1D and 0D) perovskites have shown better environmental stability.[280–282] A typical 2D perovskite can be regarded as interdigitating bulky organic bilayers intercalated by inorganic layers. The replacement of MA^+ with bulkier alkylammonium cations results in enhanced stability.[255] Inspired by this, several (quasi-) 2D perovskites having a bulky organic cation, *e.g.*, phenylethylammonium ($C_8H_9NH_3^+$, PEA^+),[283–285] 1-hexadecylammonium ($CH_3(CH_2)_{15}NH_3^+$, HDA^+),[286] have been developed (Fig. 11c). Among them, PEA-based MHPs have been widely investigated and proven that increased van der Waal's interactions[255] and reduced water adsorption energy are the key factors for the improved stability.[283] Another possibility is to have a better interaction between the A site (such as cysteamine,[287] α,ω-alkanedicarboxylates $[^-O_2C(CH_2)_4CO_2^-]$,[288,289] bipyridine[290]) and inorganic framework (Fig. 11d).[288] As supported by DFT calculations, the strong coordination between Pb atoms and adipate dianions increases the energy cost of surface hydrolysis and limits the penetration of water molecules.[289]

Meanwhile, a series of 1D and 0D MHPs with intrinsic water stability have been reported including 1D [*N*-methyldabconium] PbI_3,[291] $[(AD)Pb_2Cl_5]$,[292] $(DAO)Sn_2I_6$ (DAO = 1,8-octyldiammonium),[293] (4,4′-TMDP)Pb_2Br_6 (TMDP = trimethylenedipyridinium),[294] (4,4′-EDP)Pb_2Br_6 (EDP = ethylenedipyridinium),[294] and 0D (3-ethylbenzo[*d*]thiazol-3-ium)$_4Bi_2I_{10}$,[295] $(C_4H_9)_4NCuCl_2$.[296] The cations are summarized in Fig. 12, and the details of stability are listed in Table 4. The molecular design strategies aim to increase the ionization energy,[291] introduce cation–π interaction (Fig. 11e),[294] enhance steric hindrance effect (Fig. 11f),[292,296] or utilize hydrogen-bond-free A sites.[295] Among them, one report introduced the concept of long-range intermolecular cation–π interactions among A-site cations (4,4′-TMDP or 4,4′-EDP) of hybrid perovskites and facilitate the formation of polymer-like network, imparting water stability up to 180 days (Fig. 11e). Cation–π interaction is originated from the noncovalent interaction between the π face of aromatic ring and cation (such as alkali cations, ammonium ions),[297] which is stronger than the cation–water interactions during the decomposition of MHPs.[298] Undoubtedly, the development of intrinsic stability of MHPs in water may provide new directions and opportunities to advance the photocatalytic applications.

Besides the selection of A cations, substitution of the B sites with smaller divalent metals could reduce the lattice parameter and increase the cohesive energy, which has been reported to improve the MHP stability.[299–301] Substitution of Pb^{2+} with smaller divalent metals would also favor the formation of vacancy-ordered A_2BX_6 double perovskites with improved stability. Hamdan *et al.* synthesized a vacancy ordered halide perovskite Cs_2PtI_6 exhibiting extraordinary stability up to 1 year under ambient condition and showing stability under high temperature (350 °C), extremely acidic (pH 1) and basic (pH 13) solutions.[302] DFT calculations suggest that the improved stability is due to the strong covalent interaction of the B–X bonds in the isolated the $[BX_6]^{2-}$ clusters.[303]

Halogen anion substitution is another approach. A partial replacement of iodide with bromide was found to enhance stability and water tolerance in mixed iodide-bromide MHP compositions.[304] This is related to the suppression of oxygen incorporation and the presence of stronger hydrogen bonds

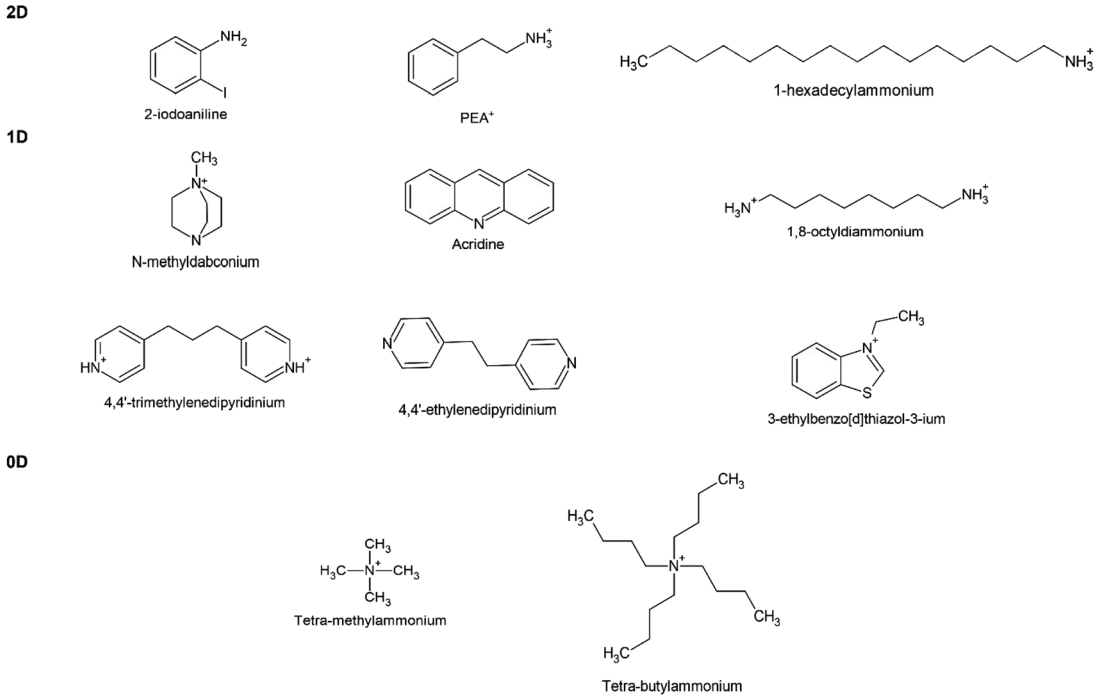

Fig. 12 Chemical structures of organic cations used for fabricating water-stable MHPs.

between the MA^+ cation and Br^- ions as the bromide content increases[305] as well as the weaker interaction of water with bromide.[306] Apart from halogen ions, pseudohalides (cyanide, cyanate, thiocyanate, selenocyanate, azide, BF_4^-, PF_6^-, BH_4^-, N_3^- and $HCOO^-$) have shown significant stability enhancement of MHPs.[307] For instance, thiocyanate (SCN)-substituted $CH_3NH_3Pb(SCN)_2I$ was shown to be more stable than pristine $CH_3NH_3PbI_3$ (for 4 h *vs.* <1.5 h) under 95% humidity.[309]

3 Photocatalytic applications

In the past seven years, water-stable MHPs have attracted much attention for numerous potential applications (Table S1 and Fig. S1†) owing to their enhanced stability and improved performance. Very recently, it has been exploited as potential photocatalysts in different reactions. In this section, we will provide an overview of these photocatalytic applications and will show lots of nice and encouraging studies for pollutant degradation, H_2 generation, CO_2 reduction and organic synthesis over water-stable MHP photocatalysts.

3.1 Pollutant degradation

Photocatalytic degradation is an attractive way to remove pollutants from wastewater and thus a great amount of work has been devoted to exploring effective photocatalysts. Aamir *et al.* firstly reported on water-stable $OHNH_3PbI_2Cl$ and $OHNH_3PbCl_3$ for photocatalytic dye degradation of Direct Yellow 27 dye under sunlight with a degree of degradation of 93.98% within 20 min and almost 100% after 55 min, respectively.[273] However, both catalysts are only UV-responsive. On the other hand, Ghosh and co-workers reported that the water-stable $MAPbBr_3$@ZIF-8 composites could degrade different pollutants (methyl orange, methyl red and nitrofurazone) under visible light (60 W LED lamp, $\lambda_{max} \sim 530$ nm) or sunlight. The composite exhibited a higher degradation for methyl orange and could degrade methyl orange up to 90% in 100 min (degradation rate constant: 0.02723 min^{-1}), shown in Fig. 13a.[215] Although the degradation rate is not high enough compared to the other materials, it can be improved by using photoactive MOFs.[310]

To alleviate the toxicity associated with Pb, some lead-free MHPs have been explored. Wu *et al.* prepared a $C_6H_4NH_2CuCl_2I$ film to degrade rhodamine B (RhB) under visible light irradiation. Degradation of 18% of RhB in 60 min was achieved (degradation rate constant: 0.003 min^{-1}). They found that the sluggish transfer rate of holes restrains photocatalytic performance of this catalyst. After coupling the photocatalyst with a hole-transporting material (CuO), the charge separation was enhanced, resulting in a degradation rate of 0.005 min^{-1}.[311] As also suggested by the study, one may enhance the overall photocatalytic activity by constructing heterojunctions that rectify electron–hole transport at the interface of two semiconductors to facilitate better charge separation and to limit photocharge recombination. A good example is a nanocomposite of PEA_2SnBr_4/g-C_3N_4 prepared *via* ball milling of the constituents. Compared with pristine g-C_3N_4, the heterojunction decreased the degradation time of methylene blue (10^{-5} M) from 90 min to 45 min (degradation rate constant: 0.078 min^{-1}) under solar light.[284] Among the so far reported photocatalysts, $DMASnI_3$ seems to show the best photocatalytic performance with a complete conversion of methyl orange (100 mg L^{-1}) in 12–15 min (degradation constant rate: ~0.13 min^{-1}) under visible light.[279]

Table 4 Summary of intrinsically water-stable MHPs[a]

Water-stable MHPs		Stability					
Materials	Methods	Medium	Characterizations	Retained PL intensity	PLQY before (after)	Observed durability	Ref.
$(C_4H_9)_4NPbI_3$	Solvent evaporation	Water (immersion)	PXRD	—	—	5 days	76
$NBCAnPbI_3\{CH_3NH_3PbI_3\}$	*In situ* synthesis	Water (immersion)	UV-vis absorption spectroscopy PXRD	—	—	30 min	73
$Rb_{0.05}Cs_{2.95}Bi_2I_9$ single crystals	Temperature lowering method	Water (immersion)	PL, PXRD, XPS and UV-vis absorption spectroscopy	~100%	17.63% (—)	24 h	308
$OHNH_3PbI_2Cl$ crystals	Solution method	Water (stirring)	UV-vis absorption spectroscopy	—	—	45 days	273
$OHNH_3PbCl_3$ crystals	Solution method	Water (stirring)	UV-vis absorption spectroscopy	—	—	45 days	273
$C_6H_4NH_2CuBr_2I$ thin film	Grinding and spin-coating	Water (immersion)	PXRD	—	—	4 h	276
$C_6H_4NH_2CuBr_2I$ thin film	—	Water (immersion)	PXRD UV-vis absorption spectroscopy	—	—	2 h	277
$(CH_3)_2NH_2SnI_3$ ($DMASnI_3$) single crystals	Temperature lowering method	Water (immersion)	PXRD	—	—	16 h	278
$DMASnI_XBr_{3-X}$ crystals	Temperature lowering method	Water (immersion)	PXRD XPS FTIR UV-vis diffuse reflectance spectroscopy	—	—	20 h	279
Mn-doped $(PEA)_2PbBr_4$ crystals	Lewis base-assisted precipitated method	Water (immersion)	High-power XRD	—	>45% (—)	45 days	283
PEA_2SnBr_4	Wet-chemistry (solvent evaporation)	Water (stirring)	PXRD ICP-OES UV-vis absorption spectroscopy XPS	—	—	4 h	284
Trifluoromethyl-modified PEA_2PbBr_4	Temperature lowering method	Water (immersion)	PL	~100%	18.11% (—)	74 days	285
$(HDA)_2PbI_4$ ($HDA^+ = CH_3(CH_2)_{15}NH_3^+$)	Modified ligand-assisted reprecipitation	Water (immersion)	PXRD PL	—	—	30 min	286
$(HCya)_2PbI_4$ (Cya = $HS(CH_2)_2NH_2$) crystals	Temperature lowering method	50% isopropanol-water (immersion)	—	—	—	>30 s	287
$[Pb_2X_2^{2+}]$ $[^-O_2C(CH_2)_4CO_2^-]$ crystals	Hydrothermal method	Boiling water, HCl solution (pH 3), and NaOH solution (pH 12)	PXRD	—	—	24 h	288

Table 4 (*Contd.*)

Water-stable MHPs		Stability					
Materials	Methods	Medium	Characterizations	Retained PL intensity	PLQY before (after)	Observed durability	Ref.
$[Pb_2X_2^{2+}]$ $[^-O_2C(CH_2)_4CO_2^-]$ crystals	Hydrothermal method	HCl solution (pH 3–6), pure water (pH 7) NaOH solution (pH 8–11) and boiling water	PXRD	—	—	24 h	289
$APbX_2$ (A = bipyridine) crystals	Ligand-assisted reprecipitation	Water (immersion)	PXRD XPS SEM	—	—	24 h	290
[*N*-Methyldabconium]PbI_3 crystals	Solvent evaporation	Water (immersion)	PXRD Dielectric permittivity	—	—	15 h	291
$[(AD)Pb_2Cl_5]$ (AD = acridine) micro-belts	Precipitation	Water (immersion)	PL PXRD SEM	~100%	7.45% (58.79%)	60 days	292
$(DAO)Sn_2I_6$ (DAO = 1,8-octyldiammonium) crystals	Temperature lowering method	Water (immersion)	XPS UV-vis absorption and Raman spectra, PXRD	—	20.3% (—)	>15 h	293
4,4′-Trimethylenedipyridinium lead bromide crystals $[(4,4'\text{-TMDP})Pb_2Br_6]$	Temperature lowering method	Water (immersion)	PL UV-vis absorption, PXRD	~100%	3.7% (—)	180 days	294
4,4′-Ethylenedipyridinium lead bromide crystals $[(4,4'\text{-EDP})Pb_2Br_6]$	Temperature lowering method	Water (immersion)	PL UV-vis absorption, PXRD	~100%	4% (—)	180 days	294
(3-Ethylbenzo[*d*]thiazol-3-ium)$_4Bi_2I_{10}$ $(EtbtBi_2I_{10})$ single crystals	Solvothermal method	Water (immersion)	PXRD	—	—	7 days	295
$(C_4H_9)_4NCuCl_2$ single crystals	Solvent evaporation	Water (immersion)	PL, XPS PXRD	98.6%	82% (—)	24 h	296
Cs_2PtI_6	Hydrothermal method	Water (immersion)	PXRD	—	—	4 h	302
$CH_3NH_3Pb(SCN)_2I$	Solvent evaporation	95% RH	UV-vis absorption spectra	—	—	4 h	309

[a] NBCAnPbI$_3$: 4-[(*N*-3-butyne)carboxyamido]anilinium lead(II) iodide; ICP-OES: inductively coupled plasma optical emission spectrometry.

3.2 H_2 evolution reaction (HER)

MHPs have also been regarded as a promising family of materials for photocatalytic HER. However, due to the constraint of water stability, previous works in MHP photocatalysts mainly focused on hydrogen generation from concentrated halide acids as summarized before.[40–47] Here, the results related to MHP-based photocatalysts for H_2 production from water are presented. The first results of H_2 evolution from water with MHPs was reported by Tao's group[278] using $DMASnI_3$, H_2 evolution from water under 300 W Xe-lamp was explored and H_2 evolution rate of 3.2 μmol g^{-1} h^{-1} was obtained. One year later, Malavasi's group observed that $DMASnBr_3$ is also highly air-resistant.[312] They proved that bare $DMASnBr_3$ photocatalyst exhibited a HER rate of 6 μmol g^{-1} h^{-1} (50 mW cm^{-2}, 1500 W Xenon lamp with UV filter), which was further improved to 11 μmol g^{-1} h^{-1} after introducing triethanolamine (TEOA) as sacrificial agent and 1 wt% Pt as co-catalyst. Later, g-C_3N_4 was introduced to further improve the HER performance by constructing heterojunctions. As shown in Fig. 13b, the $DMASnBr_3$@g-C_3N_4 (33 wt% $DMASnBr_3$) exhibited stable HER activities and reached an impressive H_2 production of 1730 μmol g^{-1} h^{-1} with an apparent quantum yield (AQY) of 6.6% (50 mW cm^{-2}, 1500 W Xenon lamp with UV filter).[313] The enhancement of photocatalytic activity is closely tied to the suitable bandgap and matched band alignment. Same strategy was extended to PEA_2SnBr_4/g-C_3N_4 and $Cs_3Bi_2Br_9$/g-C_3N_4 systems and the maximum HER rates of 1600 μmol g^{-1} h^{-1} (50 mW cm^{-2}, 1500 W Xenon lamp with UV filter) and 1050 μmol g^{-1} h^{-1} (50 mW cm^{-2}, 1500 W Xenon lamp with UV filter) were achieved, respectively.[284,314] Apart from hydrid MHPs, inorganic MHPs have also been employed as photocatalysts for HER due to their better stability in humid air.[315] Yin *et al.* prepared a series of inorganic $Cs_2Pt_xSn_{1-x}Cl_6$ ($0 \le x \le 1$) crystals *via* a hydrothermal method. The $Cs_2Pt_{0.05}Sn_{0.95}Cl_6$ catalyst exhibited good phase stability in water for at least 4 hours and obtained a rate of 16.11 μmol g^{-1} h^{-1} (300 W Xe lamp) for hydrogen evolution from water using TEOA as the sacrificial agent.[209] Encouragingly, Fei's group reported the first organolead iodide layered crystalline material $[Pb_8I_8(H_2O)_3]^{8+}[^-O_2C(CH_2)_4CO_2^-]_4$ (TJU-16) with overall photocatalytic water splitting characteristics few years ago. Combing Rh as co-catalysts, the TJU-16-$Rh_{0.22}$ exhibited a hydrogen evolution rate of 31 μmol g^{-1} h^{-1} (300 W Xenon lamp with an AM1.5 G filter) with AQY of 0.13% at 320 nm.[289]

3.3 CO_2 reduction

To alleviate environmental issues related to ever-increasing levels of CO_2 concentration in the atmosphere, photocatalytic valorization of CO_2 to useful compounds such as CO, methane, formic acid and alike have been placed in the focus of research for decades. Recently, Chen *et al.* combined water-stable perovskite-like organolead iodide $[Pb_8I_8(H_2O)_3]_8^+[^-O_2C(CH_2)_4CO_2^-]_4$ (TJU-16) with Au co-catalyst ($Au_{0.19}$/TJU-16) for photocatalytic CO_2 reduction in aqueous solution.[316] Without using any sacrificial agent, the $Au_{0.19}$/TJU-16 with loading of 0.19 wt% of Au

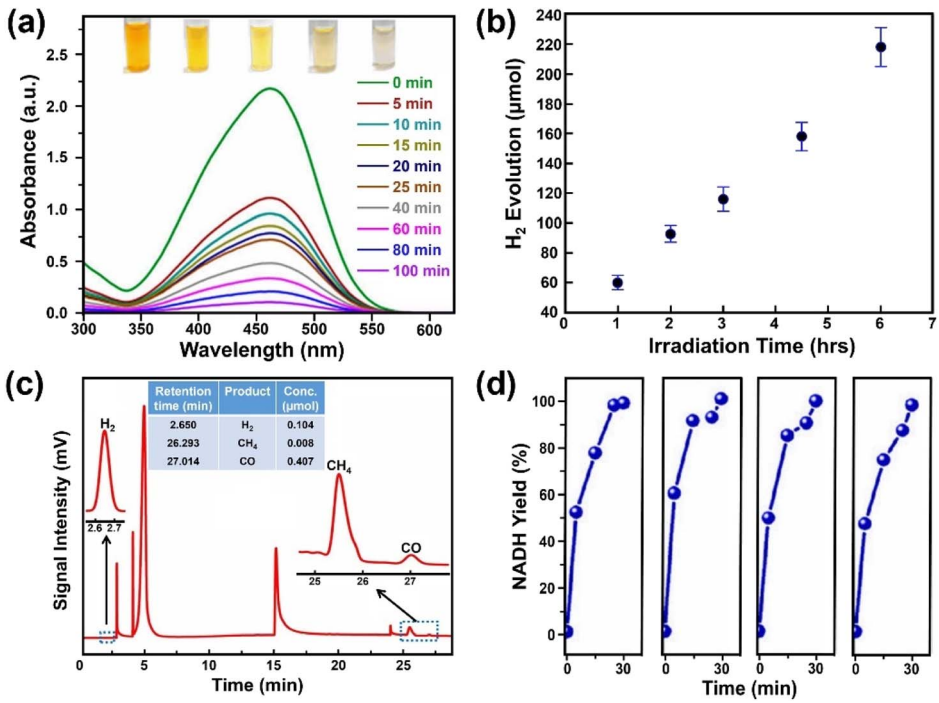

Fig. 13 Photocatalytic applications over water-stable MHPs. (a) Absorption spectra evolution of methyl orange solution degraded by $MAPbBr_3$@ZIF-8 under visible light irradiation. Adapted from ref. 215. Copyright 2019 American Chemical Society. (b) Hydrogen evolution over 33 wt% $DMASnBr_3$@g-C_3N_4 composite (1 g L^{-1}, 10% v/v triethanolamine, 3 wt% Pt) under simulated solar light. Adapted from ref. 313. Copyright 2020 John Wiley and Sons. (c) CO_2 reduction products over $CsPbBr_3$@g-C_3N_4 composite under AM1.5 G simulated sunlight. Adapted from ref. 317. Copyright 2022 Elsevier. (d) Nicotinamide adenine dinucleotide (NADH) yields over $DMASnI_3$ irradiated by blue LED lamp (wavelength of 450 nm) with four independent tests. Adapted from ref. 279. Copyright 2020 John Wiley and Sons.

nanoparticles showed the highest photocatalytic CO production rate of 2.5 μmol g^{-1} h^{-1} and CH_4 production rate of 10.1 μmol g^{-1} h^{-1} in water under AM 1.5 G simulated irradiation, achieving a solar-to-fuel conversion efficiency of 0.034%. In addition, the consumption of electrons calculated from CO and CH_4 of $Au_{0.19}$/TJU-16 is 2.2-fold of individual TJU-16. It was concluded that the improvement in the activity originated from the spatial charge accumulation and enhanced interfacial charge transfer when applying the Au co-catalyst. In another study, photocatalyst film of $CsPbBr_3$ nanoparticles coated with monolayered C_3N_4 ($CsPbBr_3$@g-C_3N_4) was found to be capable of transforming CO_2 to CO, CH_4 and H_2 (0.407, 0.104 and 0.008 μmol cm_{cat}^{-2}, respectively) in the presence of water vapor under AM1.5 G solar without using scavengers.[317] Nanoparticles of the individual phases (*i.e.*, g-C_3N_4 or $CsPbBr_3$) alone did not produce any reduction species of CO_2 (Fig. 13c). Isotopic labeling experiments confirmed the origin of products from CO_2 reduction. The improved performance was ascribed to the enhanced stability of $CsPbBr_3$ coated with the g-C_3N_4 shell as well as by the promoted separation of photocarriers at the heterojunction interface.

Doping of the photocatalyst with ionic impurities offers a further strategy to improve their optical absorption, catalytic behavior as well as carrier transport properties.[87,251] For example, Co-doped $CsPbBr_3$/Cs_4PbBr_6 NCs was demonstrated to be superior compared to its pristine counterpart for water-assisted CO_2 photoreduction with a conversion of 247 μmol g^{-1} under visible light irradiation (with CO and CH_4 as the main products). The Co-dopant is assumed to provide not only additional active sites, but it is also believed to be responsible for altering the adsorption energies of reactants and intermediates thus influencing the reaction pathways.

3.4 Organic synthesis

Photocatalytic synthesis of organic compounds is another fascinating field to offer environmentally benign and cost-effective routes. Although numerous works have been done with MHPs for organic synthesis, such as C–X (X = C, N, O, P) formation, carbon–carbon cleavage and carbon–hydrogen activation, all these photocatalytic reactions are limited to nonpolar solvent systems.[30–33] To broaden their applications in aqueous system, a prerequisite factor is to utilize water-stable MHPs. Ju *et al.* firstly extended the organic synthesis to aqueous solution with $DMASnI_xBr_{3-x}$ for photoenzyme catalysis.[279] The nicotinamide adenine dinucleotide (NADH) yield was nearly 100% within only 30 min and exhibited stable reproducibility in four tests under blue LED irradiation (Fig. 13d). 320 μM formic acid can be obtained over a period of 60 min in the photoenzymatic reaction, suggesting an efficient photocatalytic process in artificial photosynthesis.

4 Challenges and prospects

In this review, we summarize the significant advances in the development and applications of water-stable MHPs. To date, the water stability of MHPs has been achieved by surface engineering, common-ion effect and intrinsically stable MHPs. As an emerging class of photocatalysts, the photocatalytic study of water-stable MHPs is still in their infancy. Several challenges and future research directions related to water-stable MHPs are identified as follows:

(1) Although various strategies have been proposed to obtain water stability of MHPs, to realize their photocatalytic applications, studies should be further focused on the charge carrier transport properties by exploring novel MHPs with intrinsic water compatibility (quasi-3D and 2D MHPs) and/or employing surface passivation that can protect MHPs from water while preserving good carrier transport features.[318–323] For example, constructing a MHP@shell core–shell heterostructure is a highly promising way to hit two birds with one stone. By bringing MHPs with semiconducting/conductive shell, not only new catalytically active sites[324] or protective coatings[325] can be introduced by the second phase, but more importantly rectifying interfaces may be obtained.

(2) While some water-stable MHP based photocatalytic systems have shown good photocatalytic activity in the degradation of organic dyes, more challenging and highly relevant fields such as hydrogen evolution and activation/valorization of CO_2 are still in their early stages of development, and catalysts exhibit lower photocatalytic performance compared to traditional photocatalysts.[326] One possibility for the inferior activity might lie in the severe surface charge recombination.[327] In this regard, constructing a close–contact interface among MHP-based composites, which benefits the sufficient transfer and rectification of photogenerated charges, is highly desirable.[328–330] It has been proven that chemical modification or *in situ* synthesis can result in an intimate heterointerface.[151,325,330,331] Therefore, in the future, it is plausible to expect new avenues in this direction as well.

(3) Another vital direction of research is towards an in-depth understanding of reaction mechanisms over MHP-based photocatalysts, as the contemporary results are not entirely coherent and conclusive. Taking CO_2 reduction reaction as an example, there are debates over the CO_2 adsorption sites on bismuth-based $A_3Bi_2I_9$ (A = Rb^+, Cs^+ or MA^+)[332–335] and the origin of products (photocatalysis[317] or photolysis[336,337]). The photocatalytic HER reaction mechanism over $DMASnBr_3$ is also not exhaustive. It is reported that the binding energy of electron polarons over $DMASnBr_3$ surface dominates the HER activity, but the specific role of electron polarons, as driving force or trapping charges, needs further investigation.[338] In this regard, combining analytics, such as *in situ* Fourier-transform infrared spectroscopy, *in situ* Raman, *etc.*, with theoretical investigations, will provide new insights in understanding the mechanisms involved and thereby to the design of water-stable and efficient MHPs.

Author contributions

H. Z.: conceptualization, formal analysis, investigation, writing – original draft; K. K.: supervision, funding acquisition, resources, writing – review & editing; S. O.: supervision, funding acquisition, resources, writing – review & editing.

Conflicts of interest

There are no conflicts to declare.

Acknowledgements

This work is supported by the Kvantum Institute Emerging Project (Charge carrier recombination dynamics in semiconductor materials) at the University of Oulu. H. Z. acknowledges the financial support of Tauno Tönning Foundation (grant no. 20210036) and University of Oulu Scholarship Fund (grant no. 20220010).

Notes and references

1 L. Gibson, E. N. Wilman and W. F. Laurance, *Trends Ecol. Evol.*, 2017, **32**, 922–935.
2 N. Kannan and D. Vakeesan, *Renewable Sustainable Energy Rev.*, 2016, **62**, 1092–1105.
3 J. H. Kim, D. Hansora, P. Sharma, J.-W. Jang and J. S. Lee, *Chem. Soc. Rev.*, 2019, **48**, 1908–1971.
4 H. Nishiyama, T. Yamada, M. Nakabayashi, Y. Maehara, M. Yamaguchi, Y. Kuromiya, Y. Nagatsuma, H. Tokudome, S. Akiyama, T. Watanabe, R. Narushima, S. Okunaka, N. Shibata, T. Takata, T. Hisatomi and K. Domen, *Nature*, 2021, **598**, 304–307.
5 P. Zhou, I. A. Navid, Y. Ma, Y. Xiao, P. Wang, Z. Ye, B. Zhou, K. Sun and Z. Mi, *Nature*, 2023, **613**, 66–70.
6 B. A. Pinaud, J. D. Benck, L. C. Seitz, A. J. Forman, Z. Chen, T. G. Deutsch, B. D. James, K. N. Baum, G. N. Baum, S. Ardo, H. Wang, E. Miller and T. F. Jaramillo, *Energy Environ. Sci.*, 2013, **6**, 1983.
7 Y.-H. Song, J. S. Yoo, E. K. Ji, C. W. Lee, G. S. Han, H. S. Jung and D.-H. Yoon, *Chem. Eng. J.*, 2016, **306**, 791–795.
8 S. Chen, T. Takata and K. Domen, *Nat. Rev. Mater.*, 2017, **2**, 17050.
9 N. A. Romero and D. A. Nicewicz, *Chem. Rev.*, 2016, **116**, 10075–10166.
10 J. Twilton, C. Le, P. Zhang, M. H. Shaw, R. W. Evans and D. W. C. MacMillan, *Nat. Rev. Chem*, 2017, **1**, 0052.
11 J. Schneider, M. Matsuoka, M. Takeuchi, J. Zhang, Y. Horiuchi, M. Anpo and D. W. Bahnemann, *Chem. Rev.*, 2014, **114**, 9919–9986.
12 Y. Ma, X. Wang, Y. Jia, X. Chen, H. Han and C. Li, *Chem. Rev.*, 2014, **114**, 9987–10043.
13 G. Liao, Y. Gong, L. Zhang, H. Gao, G.-J. Yang and B. Fang, *Energy Environ. Sci.*, 2019, **12**, 2080–2147.
14 A. Kumar Singh, C. Das and A. Indra, *Coord. Chem. Rev.*, 2022, **465**, 214516.
15 V.-H. Nguyen, H. H. Do, T. Van Nguyen, P. Singh, P. Raizada, A. Sharma, S. S. Sana, A. N. Grace, M. Shokouhimehr, S. H. Ahn, C. Xia, S. Y. Kim and Q. Van Le, *Sol. Energy*, 2020, **211**, 584–599.
16 A. Hossain, A. Bhattacharyya and O. Reiser, *Science*, 2019, **364**, eaav9713.
17 F. E. Osterloh, *Chem. Mater.*, 2008, **20**, 35–54.
18 K. Maeda and K. Domen, *J. Phys. Chem. Lett.*, 2010, **1**, 2655–2661.
19 M. Rahman, H. Tian and T. Edvinsson, *Angew. Chem., Int. Ed.*, 2020, **59**, 16278–16293.
20 A. Kojima, K. Teshima, Y. Shirai and T. Miyasaka, *J. Am. Chem. Soc.*, 2009, **131**, 6050–6051.
21 H. Min, D. Y. Lee, J. Kim, G. Kim, K. S. Lee, J. Kim, M. J. Paik, Y. K. Kim, K. S. Kim, M. G. Kim, T. J. Shin and S. Il Seok, *Nature*, 2021, **598**, 444–450.
22 G. Xing, N. Mathews, S. Sun, S. S. Lim, Y. M. Lam, M. Grätzel, S. Mhaisalkar and T. C. Sum, *Science*, 2013, **342**, 344–347.
23 M. A. Green, A. Ho-Baillie and H. J. Snaith, *Nat. Photonics*, 2014, **8**, 506–514.
24 Q. Dong, Y. Fang, Y. Shao, P. Mulligan, J. Qiu, L. Cao and J. Huang, *Science*, 2015, **347**, 967–970.
25 C. Wehrenfennig, G. E. Eperon, M. B. Johnston, H. J. Snaith and L. M. Herz, *Adv. Mater.*, 2014, **26**, 1584–1589.
26 P. Chen, W. Ong, Z. Shi, X. Zhao and N. Li, *Adv. Funct. Mater.*, 2020, **30**, 1909667.
27 Y. Zhou and Y. Zhao, *Energy Environ. Sci.*, 2019, **12**, 1495–1511.
28 S. Park, W. J. Chang, C. W. Lee, S. Park, H.-Y. Ahn and K. T. Nam, *Nat. Energy*, 2017, **2**, 16185.
29 P. C. K. Vesborg, *Nat. Energy*, 2017, **2**, 16205.
30 Y. Lin, J. Guo, J. San Martin, C. Han, R. Martinez and Y. Yan, *Chem. –Eur. J.*, 2020, **26**, 13118–13136.
31 M. Corti, S. Bonomi, R. Chiara, L. Romani, P. Quadrelli and L. Malavasi, *Inorganics*, 2021, **9**, 56.
32 M. Zhang, W. Sun, H. Lv and Z.-H. Zhang, *Curr. Opin. Green Sustainable Chem.*, 2021, **27**, 100390.
33 V. Murugesh and S. P. Singh, *Chem. Rec.*, 2020, **20**, 1181–1197.
34 S. Shyamal and N. Pradhan, *J. Phys. Chem. Lett.*, 2020, **11**, 6921–6934.
35 S. Trivedi, D. Prochowicz, A. Kalam, M. M. Tavakoli and P. Yadav, *Renewable Sustainable Energy Rev.*, 2021, **145**, 111047.
36 M. A. Raza, F. Li, M. Que, L. Zhu and X. Chen, *Mater. Adv.*, 2021, **2**, 7187–7209.
37 X. Zhang, R. Tang, F. Li, R. Zheng and J. Huang, *Sol. RRL*, 2022, **6**, 2101058.
38 J. Wang, Y. Shi, Y. Wang and Z. Li, *ACS Energy Lett.*, 2022, **7**, 2043–2059.
39 C. B. Hiragond, N. S. Powar and S.-I. In, *Nanomaterials*, 2020, **10**, 2569.
40 L. Romani and L. Malavasi, *ACS Omega*, 2020, **5**, 25511–25519.
41 S. Purohit, K. L. Yadav and S. Satapathi, *Adv. Mater. Interfaces*, 2022, **9**, 2200058.
42 V. Armenise, S. Colella, F. Fracassi and A. Listorti, *Nanomaterials*, 2021, **11**, 433.
43 H. Huang, B. Pradhan, J. Hofkens, M. B. J. Roeffaers and J. A. Steele, *ACS Energy Lett.*, 2020, **5**, 1107–1123.
44 J. Chen, C. Dong, H. Idriss, O. F. Mohammed and O. M. Bakr, *Adv. Energy Mater.*, 2020, **10**, 1902433.
45 Y. Xu, M. Cao and S. Huang, *Nano Res.*, 2021, **14**, 3773–3794.

46 J. Luo, W. Zhang, H. Yang, Q. Fan, F. Xiong, S. Liu, D. Li and B. Liu, *EcoMat*, 2021, **3**, eom2.12079.
47 S. Pan, J. Li, Z. Wen, R. Lu, Q. Zhang, H. Jin, L. Zhang, Y. Chen and S. Wang, *Adv. Energy Mater.*, 2022, **12**, 2004002.
48 H. Zhou, Q. Chen, G. Li, S. Luo, T. B. Song, H. S. Duan, Z. Hong, J. You, Y. Liu and Y. Yang, *Science*, 2014, **345**, 542–546.
49 N. Tripathi, M. Yanagida, Y. Shirai, T. Masuda, L. Han and K. Miyano, *J. Mater. Chem. A*, 2015, **3**, 12081–12088.
50 W. Oh, S. Bae, S. Kim, N. Park, S.-I. Chan, H. Choi, H. Hwang and D. Kim, *Microelectron. Reliab.*, 2019, **100–101**, 113392.
51 C. Müller, T. Glaser, M. Plogmeyer, M. Sendner, S. Döring, A. A. Bakulin, C. Brzuska, R. Scheer, M. S. Pshenichnikov, W. Kowalsky, A. Pucci and R. Lovrinčić, *Chem. Mater.*, 2015, **27**, 7835–7841.
52 J. M. Frost, K. T. Butler, F. Brivio, C. H. Hendon, M. van Schilfgaarde and A. Walsh, *Nano Lett.*, 2014, **14**, 2584–2590.
53 Y. Li, X. Xu, C. Wang, C. Wang, F. Xie, J. Yang and Y. Gao, *J. Phys. Chem. C*, 2015, **119**, 23996–24002.
54 E. Mosconi, J. M. Azpiroz and F. De Angelis, *Chem. Mater.*, 2015, **27**, 4885–4892.
55 A. M. A. Leguy, Y. Hu, M. Campoy-Quiles, M. I. Alonso, O. J. Weber, P. Azarhoosh, M. van Schilfgaarde, M. T. Weller, T. Bein, J. Nelson, P. Docampo and P. R. F. Barnes, *Chem. Mater.*, 2015, **27**, 3397–3407.
56 J. Yang, B. D. Siempelkamp, D. Liu and T. L. Kelly, *ACS Nano*, 2015, **9**, 1955–1963.
57 Z. Song, A. Abate, S. C. Watthage, G. K. Liyanage, A. B. Phillips, U. Steiner, M. Graetzel and M. J. Heben, *Adv. Energy Mater.*, 2016, **6**, 1600846.
58 G. E. Eperon, S. N. Habisreutinger, T. Leijtens, B. J. Bruijnaers, J. J. van Franeker, D. W. DeQuilettes, S. Pathak, R. J. Sutton, G. Grancini, D. S. Ginger, R. A. J. Janssen, A. Petrozza and H. J. Snaith, *ACS Nano*, 2015, **9**, 9380–9393.
59 G. Grancini, V. D'Innocenzo, E. R. Dohner, N. Martino, A. R. Srimath Kandada, E. Mosconi, F. De Angelis, H. I. Karunadasa, E. T. Hoke and A. Petrozza, *Chem. Sci.*, 2015, **6**, 7305–7310.
60 C. Zheng and O. Rubel, *J. Phys. Chem. C*, 2019, **123**, 19385–19394.
61 S. Sun, D. Yuan, Y. Xu, A. Wang and Z. Deng, *ACS Nano*, 2016, **10**, 3648–3657.
62 H. Zhang, M. K. Nazeeruddin and W. C. H. Choy, *Adv. Mater.*, 2019, **31**, 1805702.
63 J. De Roo, M. Ibáñez, P. Geiregat, G. Nedelcu, W. Walravens, J. Maes, J. C. Martins, I. Van Driessche, M. V. Kovalenko and Z. Hens, *ACS Nano*, 2016, **10**, 2071–2081.
64 Y. Wei, Z. Cheng and J. Lin, *Chem. Soc. Rev.*, 2019, **48**, 310–350.
65 X. Du, R. Qiu, T. Zou, X. Chen, H. Chen and H. Zhou, *Adv. Mater. Interfaces*, 2019, **6**, 1900413.
66 A. Ciccioli, R. Panetta, A. Luongo, B. Brunetti, S. Vecchio Ciprioti, M. L. Mele and A. Latini, *Phys. Chem. Chem. Phys.*, 2019, **21**, 24768–24777.
67 B. Parida, I. S. Jin and J. W. Jung, *Chem. Mater.*, 2021, **33**, 5850–5858.
68 Y. Miao, M. Zheng, H. Wang, C. Chen, X. Ding, C. Wu, B. Wang, M. Zhai, X. Yang and M. Cheng, *J. Power Sources*, 2021, **492**, 229621.
69 I. Poli, S. Eslava and P. Cameron, *J. Mater. Chem. A*, 2017, **5**, 22325–22333.
70 Z. Xu, R. Chen, Y. Wu, R. He, J. Yin, W. Lin, B. Wu, J. Li and N. Zheng, *J. Mater. Chem. A*, 2019, **7**, 26849–26857.
71 S. Yang, Y. Wang, P. Liu, Y.-B. Cheng, H. J. Zhao and H. G. Yang, *Nat. Energy*, 2016, **1**, 15016.
72 Y. Guo, S. Apergi, N. Li, M. Chen, C. Yin, Z. Yuan, F. Gao, F. Xie, G. Brocks, S. Tao and N. Zhao, *Nat. Commun.*, 2021, **12**, 644.
73 S. Sasmal, S. Valiyaveettil, A. P. Upadhyay, R. G. S. Pala, S. Sivakumar, C. S. Sundar and D. Sornadurai, *MRS Commun.*, 2018, **8**, 289–296.
74 M. Aamir, A. F. Butt, M. D. Khan, M. Sher, A. Iqbal, M. A. Malik, U. Jabeen and J. Akhtar, *Optik*, 2020, **207**, 163828.
75 X. Liu, X. Wang, T. Zhang, Y. Miao, Z. Qin, Y. Chen and Y. Zhao, *Angew. Chem., Int. Ed.*, 2021, **60**, 12351–12355.
76 H. Wang, Z. Zhang, J. V. Milić, L. Tan, Z. Wang, R. Chen, X. Jing, C. Yi, Y. Ding, Y. Li, Y. Zhao, X. Zhang, A. Hagfeldt, M. Grätzel and J. Luo, *Adv. Energy Mater.*, 2021, **11**, 2101082.
77 Q. A. Akkerman, G. Rainò, M. V. Kovalenko and L. Manna, *Nat. Mater.*, 2018, **17**, 394–405.
78 H. Huang, B. Chen, Z. Wang, T. F. Hung, A. S. Susha, H. Zhong and A. L. Rogach, *Chem. Sci.*, 2016, **7**, 5699–5703.
79 H. Wu, S. Lin, R. Wang, X. You and Y. Chi, *Nanoscale*, 2019, **11**, 5557–5563.
80 S. Liu, L. Yuan, Y. Zhao, Y. Chen, W. Xiang and X. Liang, *J. Alloys Compd.*, 2019, **806**, 1022–1028.
81 C.-H. Lu, S.-W. Kuo, C.-F. Huang and F.-C. Chang, *J. Phys. Chem. C*, 2009, **113**, 3517–3524.
82 B. P. Kennedy and A. B. P. Lever, *Can. J. Chem.*, 1972, **50**, 3488–3507.
83 H. Plenio, *ChemBioChem*, 2004, **5**, 650–655.
84 C. J. Drummond, G. Georgaklis and D. Y. C. Chan, *Langmuir*, 1996, **12**, 2617–2621.
85 K. C. Hoang and S. Mecozzi, *Langmuir*, 2004, **20**, 7347–7350.
86 Z. Li, Q. Hu, Z. Tan, Y. Yang, M. Leng, X. Liu, C. Ge, G. Niu and J. Tang, *ACS Appl. Mater. Interfaces*, 2018, **10**, 43915–43922.
87 Y. Mu, W. Zhang, X. Guo, G. Dong, M. Zhang and T. Lu, *ChemSusChem*, 2019, **12**, 4769–4774.
88 L. Yang, T. Wang, Q. Min, B. Liu, Z. Liu, X. Fan, J. Qiu, X. Xu, J. Yu and X. Yu, *ACS Omega*, 2019, **4**, 6084–6091.
89 A. Gericke and H. Hühnerfuss, *Thin Solid Films*, 1994, **245**, 74–82.
90 T. Lu, Y. Zhu, Y. Kang, J. Xu and A. Wang, *Int. J. Biol. Macromol.*, 2021, **193**, 1676–1684.
91 Y. Chang, Y. J. Yoon, G. Li, E. Xu, S. Yu, C.-H. Lu, Z. Wang, Y. He, C. H. Lin, B. K. Wagner, V. V. Tsukruk, Z. Kang, N. Thadhani, Y. Jiang and Z. Lin, *ACS Appl. Mater. Interfaces*, 2018, **10**, 37267–37276.

92 B. Shu, Y. Chang, L. Dong, L. Chen, H. Wang, S. Yang, J. Zhang, X. Cheng and D. Yu, *J. Lumin.*, 2021, **234**, 117962.
93 C. G. Sanjayan, M. S. Jyothi, M. Sakar and R. G. Balakrishna, *J. Colloid Interface Sci.*, 2021, **603**, 758–770.
94 L. Gomez, C. de Weerd, J. L. Hueso and T. Gregorkiewicz, *Nanoscale*, 2017, **9**, 631–636.
95 A. Jana, K. N. Lawrence, M. B. Teunis, M. Mandal, A. Kumbhar and R. Sardar, *Chem. Mater.*, 2016, **28**, 1107–1120.
96 S. Biswas, S. Akhil, N. Kumar, M. Palabathuni, R. Singh, V. G. V. Dutt and N. Mishra, *J. Phys. Chem. Lett.*, 2023, **14**, 1910–1917.
97 Z. Chen, Y. Hu, J. Wang, Q. Shen, Y. Zhang, C. Ding, Y. Bai, G. Jiang, Z. Li and N. Gaponik, *Chem. Mater.*, 2020, **32**, 1517–1525.
98 J.-C. Wang, N. Li, A. M. Idris, J. Wang, X. Du, Z. Pan and Z. Li, *Sol. RRL*, 2021, **5**, 1–8.
99 J. G. Smith and P. K. Jain, *J. Am. Chem. Soc.*, 2016, **138**, 6765–6773.
100 Y. Yuan, H. Zhu, K. Hills-Kimball, T. Cai, W. Shi, Z. Wei, H. Yang, Y. Candler, P. Wang, J. He and O. Chen, *Angew. Chem., Int. Ed.*, 2020, **59**, 22563–22569.
101 M. Zhao, D. Ding, F. Yang, D. Wang, J. Lv, W. Hu, C. Lu and Z. Tang, *Nano Res.*, 2017, **10**, 1249–1257.
102 J. Chang, Y. Ogomi, C. Ding, Y. H. Zhang, T. Toyoda, S. Hayase, K. Katayama and Q. Shen, *Phys. Chem. Chem. Phys.*, 2017, **19**, 6358–6367.
103 H. Lu, X. Zhu, C. Miller, J. San Martin, X. Chen, E. M. Miller, Y. Yan and M. C. Beard, *J. Chem. Phys.*, 2019, **151**, 204305.
104 J. Pan, Y. Shang, J. Yin, M. De Bastiani, W. Peng, I. Dursun, L. Sinatra, A. M. El-Zohry, M. N. Hedhili, A.-H. Emwas, O. F. Mohammed, Z. Ning and O. M. Bakr, *J. Am. Chem. Soc.*, 2018, **140**, 562–565.
105 S. Han, H. Zhang, R. Wang and Q. He, *Mater. Sci. Semicond. Process.*, 2021, **131**, 105847.
106 C. Lin, J. Li, N. She, S. Huang, C. Huang, I. Wang, F. Tsai, C. Wei, T. Lee, D. Wang, C. Wen, S. Li, A. Yabushita, C. Luo, C. Chen and C. Chen, *Small*, 2022, **18**, 2107881.
107 C. Gao, F. Zhang, X. Gu, J. Huang, K. Wang, S. Zhang, S. Liu and Q. Tian, *ACS Appl. Energy Mater.*, 2021, **4**, 4021–4028.
108 C. Zhao, Z. He, P. Wangyang, J. Tan, C. Shi, A. Pan, L. He and Y. Liu, *ACS Appl. Nano Mater.*, 2022, **5**, 13737–13744.
109 J. Chen, S.-G. Kim, X. Ren, H. S. Jung and N.-G. Park, *J. Mater. Chem. A*, 2019, **7**, 4977–4987.
110 W. Zhang, Q. Li and Z. Li, *Adv. Mater. Interfaces*, 2022, **9**, 2101881.
111 H. Zhang, Y. Wu, C. Shen, E. Li, C. Yan, W. Zhang, H. Tian, L. Han and W. Zhu, *Adv. Energy Mater.*, 2019, **9**, 1803573.
112 Y. Yang, J. Liang, Z. Zhang, C. Tian, X. Wu, Y. Zheng, Y. Huang, J. Wang, Z. Zhou, M. He, Z. Chen and C. Chen, *ChemSusChem*, 2022, **15**, e202102474.
113 Y. Li, M. Cai, M. Shen, Y. Cai and R.-J. Xie, *J. Mater. Chem. C*, 2022, **10**, 8356–8363.
114 Q. Chen, X. Yang, Y. Zhou and B. Song, *New J. Chem.*, 2021, **45**, 15118–15130.
115 H. Wu, S. Wang, F. Cao, J. Zhou, Q. Wu, H. Wang, X. Li, L. Yin and X. Yang, *Chem. Mater.*, 2019, **31**, 1936–1940.
116 A. F. Carrizo, G. K. Belmonte, F. S. Santos, C. W. Backes, G. B. Strapasson, L. C. Schmidt, F. S. Rodembusch and D. E. Weibel, *ACS Appl. Mater. Interfaces*, 2021, **13**, 59252–59262.
117 B. Yu, S. Liang, F. Zhang, Z. Li, B. Liu and X. Ding, *Photonics Res.*, 2021, **9**, 1559.
118 S. Wang, Z. Zhang, Z. Tang, C. Su, W. Huang, Y. Li and G. Xing, *Nano Energy*, 2021, **82**, 105712.
119 Y. Yang and H. Zhao, *Appl. Surf. Sci.*, 2022, **577**, 151895.
120 J. Han, M. Sharipov, S. Hwang, Y. Lee, B. T. Huy and Y.-I. Lee, *Sci. Rep.*, 2022, **12**, 3147.
121 H. C. Yoon, H. Kang, S. Lee, J. H. Oh, H. Yang and Y. R. Do, *ACS Appl. Mater. Interfaces*, 2016, **8**, 18189–18200.
122 J. Ren, X. Dong, G. Zhang, T. Li and Y. Wang, *New J. Chem.*, 2017, **41**, 13961–13967.
123 Y. Zhang, B. Zhang, Y. Fu, Y. Han, T. Zhang, L. Zhang, J. Guo and X. Zhang, *J. Mater. Chem. C*, 2022, **10**, 8609–8616.
124 H. Wang, H. Lin, X. Piao, P. Tian, M. Fang, X. An, C. Luo, R. Qi, Y. Chen and H. Peng, *J. Mater. Chem. C*, 2017, **5**, 12044–12049.
125 S. Kango, S. Kalia, A. Celli, J. Njuguna, Y. Habibi and R. Kumar, *Prog. Polym. Sci.*, 2013, **38**, 1232–1261.
126 S. Masi, A. Rizzo, F. Aiello, F. Balzano, G. Uccello-Barretta, A. Listorti, G. Gigli and S. Colella, *Nanoscale*, 2015, **7**, 18956–18963.
127 B. Erman and P. J. Flory, *Macromolecules*, 1986, **19**, 2342–2353.
128 C. Carrillo-Carrión, P. del Pino and B. Pelaz, *Appl. Mater. Today*, 2019, **15**, 562–569.
129 Y. Wang, J. He, H. Chen, J. Chen, R. Zhu, P. Ma, A. Towers, Y. Lin, A. J. Gesquiere, S. Wu and Y. Dong, *Adv. Mater.*, 2016, **28**, 10710–10717.
130 Y. Wei, X. Deng, Z. Xie, X. Cai, S. Liang, P. Ma, Z. Hou, Z. Cheng and J. Lin, *Adv. Funct. Mater.*, 2017, **27**, 1703535.
131 J. An, M. Chen, G. Liu, Y. Hu, R. Chen, Y. Lyu, S. Sharma and Y. Liu, *Anal. Bioanal. Chem.*, 2021, **413**, 1739–1747.
132 Y. Xin, H. Zhao and J. Zhang, *ACS Appl. Mater. Interfaces*, 2018, **10**, 4971–4980.
133 H. Sun, Z. Yang, M. Wei, W. Sun, X. Li, S. Ye, Y. Zhao, H. Tan, E. L. Kynaston, T. B. Schon, H. Yan, Z.-H. Lu, G. A. Ozin, E. H. Sargent and D. S. Seferos, *Adv. Mater.*, 2017, **29**, 1701153.
134 V. A. Hintermayr, C. Lampe, M. Löw, J. Roemer, W. Vanderlinden, M. Gramlich, A. X. Böhm, C. Sattler, B. Nickel, T. Lohmüller and A. S. Urban, *Nano Lett.*, 2019, **19**, 4928–4933.
135 J. Zhang, P. Jiang, Y. Wang, X. Liu, J. Ma and G. Tu, *ACS Appl. Mater. Interfaces*, 2020, **12**, 3080–3085.
136 Q. Zhou, Z. Bai, W. Lu, Y. Wang, B. Zou and H. Zhong, *Adv. Mater.*, 2016, **28**, 9163–9168.
137 G. Jiang, C. Guhrenz, A. Kirch, L. Sonntag, C. Bauer, X. Fan, J. Wang, S. Reineke, N. Gaponik and A. Eychmüller, *ACS Nano*, 2019, **13**, 10386–10396.
138 Z. Lu, Y. Li, Y. Xue, W. Zhou, S. Bayer, I. D. Williams, A. L. Rogach and S. Nagl, *ACS Appl. Nano Mater.*, 2022, **5**, 5025–5034.

139 Y. Shu, Y. Wang, J. Guan, Z. Ji, Q. Xu and X. Hu, *Anal. Chem.*, 2022, **94**, 5415–5424.
140 H. Zhang, X. Wang, Q. Liao, Z. Xu, H. Li, L. Zheng and H. Fu, *Adv. Funct. Mater.*, 2017, **27**, 1604382.
141 J. Hai, H. Li, Y. Zhao, F. Chen, Y. Peng and B. Wang, *Chem. Commun.*, 2017, **53**, 5400–5403.
142 A. Pramanik, K. Gates, S. Patibandla, D. Davis, S. Begum, R. Iftekhar, S. Alamgir, S. Paige, M. M. Porter and P. C. Ray, *ACS Appl. Bio Mater.*, 2019, **2**, 5872–5879.
143 S. N. Raja, Y. Bekenstein, M. A. Koc, S. Fischer, D. Zhang, L. Lin, R. O. Ritchie, P. Yang and A. P. Alivisatos, *ACS Appl. Mater. Interfaces*, 2016, **8**, 35523–35533.
144 J. Xi, Y. Wu, W. Chen, Q. Li, J. Li, Y. Shen, H. Chen, G. Xu, H. Yang, Z. Chen, N. Li, J. Zhu, Y. Li and Y. Li, *Nano Energy*, 2022, **93**, 106846.
145 Z. Zhang, L. Liu, H. Huang, L. Li, Y. Wang, J. Xu and J. Xu, *Appl. Surf. Sci.*, 2020, **526**, 146735.
146 Z. Zhang, L. Li, L. Liu, X. Xiao, H. Huang and J. Xu, *J. Phys. Chem. C*, 2020, **124**, 22228–22234.
147 F.-J. Kahle, C. Saller, A. Köhler and P. Strohriegl, *Adv. Energy Mater.*, 2017, **7**, 1700306.
148 T. Xu, J. Stevens, J. A. Villa, J. T. Goldbach, K. W. Guarini, C. T. Black, C. J. Hawker and T. P. Russell, *Adv. Funct. Mater.*, 2003, **13**, 698–702.
149 Y. Liu, Z. Wang, S. Liang, Z. Li, M. Zhang, H. Li and Z. Lin, *Nano Lett.*, 2019, **19**, 9019–9028.
150 K. Manokruang and E. Manias, *Mater. Lett.*, 2009, **63**, 1144–1147.
151 W. Hu, Z. Wen, X. Yu, P. Qian, W. Lian, X. Li, Y. Shang, X. Wu, T. Chen, Y. Lu, M. Wang and S. Yang, *Adv. Sci.*, 2021, **8**, 2004662.
152 F. Wang, M. Endo, S. Mouri, Y. Miyauchi, Y. Ohno, A. Wakamiya, Y. Murata and K. Matsuda, *Nanoscale*, 2016, **8**, 11882–11888.
153 S. Kundu and T. L. Kelly, *Mater. Chem. Front.*, 2018, **2**, 81–89.
154 C. Wu, K. Wang, Y. Yan, D. Yang, Y. Jiang, B. Chi, J. Liu, A. R. Esker, J. Rowe, A. J. Morris, M. Sanghadasa and S. Priya, *Adv. Funct. Mater.*, 2019, **29**, 1804419.
155 M. Meyns, M. Perálvarez, A. Heuer-Jungemann, W. Hertog, M. Ibáñez, R. Nafria, A. Genç, J. Arbiol, M. V. Kovalenko, J. Carreras, A. Cabot and A. G. Kanaras, *ACS Appl. Mater. Interfaces*, 2016, **8**, 19579–19586.
156 A. F. Demirörs, A. van Blaaderen and A. Imhof, *Langmuir*, 2010, **26**, 9297–9303.
157 A. Loiudice, S. Saris, E. Oveisi, D. T. L. Alexander and R. Buonsanti, *Angew. Chem., Int. Ed.*, 2017, **56**, 10696–10701.
158 H. Yu, X. Xu, H. Liu, Y. Wan, X. Cheng, J. Chen, Y. Ye and L. Dai, *ACS Nano*, 2020, **14**, 552–558.
159 H. Hu, L. Wu, Y. Tan, Q. Zhong, M. Chen, Y. Qiu, D. Yang, B. Sun, Q. Zhang and Y. Yin, *J. Am. Chem. Soc.*, 2018, **140**, 406–412.
160 H. Liu, Y. Tan, M. Cao, H. Hu, L. Wu, X. Yu, L. Wang, B. Sun and Q. Zhang, *ACS Nano*, 2019, **13**, 5366–5374.
161 Q. Zhong, M. Cao, H. Hu, D. Yang, M. Chen, P. Li, L. Wu and Q. Zhang, *ACS Nano*, 2018, **12**, 8579–8587.
162 Y.-T. Hsieh, Y.-F. Lin and W.-R. Liu, *ACS Appl. Mater. Interfaces*, 2020, **12**, 58049–58059.
163 Z. Li, C. Song, J. Li, G. Liang, L. Rao, S. Yu, X. Ding, Y. Tang, B. Yu, J. Ou, U. Lemmer and G. Gomard, *Adv. Mater. Technol.*, 2020, **5**, 1900941.
164 P. M. Talianov, O. O. Peltek, M. Masharin, S. Khubezhov, M. A. Baranov, A. Drabavičius, A. S. Timin, L. E. Zelenkov, A. P. Pushkarev, S. V. Makarov and M. V. Zyuzin, *J. Phys. Chem. Lett.*, 2021, **12**, 8991–8998.
165 F. Gao, W. Yang, X. Liu, Y. Li, W. Liu, H. Xu and Y. Liu, *Chem. Eng. J.*, 2021, **407**, 128001.
166 H. Wu, Y. Chen, W. Zhang, M. S. Khan and Y. Chi, *ACS Appl. Nano Mater.*, 2021, **4**, 11791–11800.
167 S. Li, D. Lei, W. Ren, X. Guo, S. Wu, Y. Zhu, A. L. Rogach, M. Chhowalla and A. K. Y. Jen, *Nat. Commun.*, 2020, **11**, 1192.
168 C.-Y. You, F.-M. Li, L.-H. Lin, J.-S. Lin, Q.-Q. Chen, P. M. Radjenovic, Z.-Q. Tian and J.-F. Li, *Nano Energy*, 2020, **71**, 104554.
169 Y. Huang, F. Li, L. Qiu, F. Lin, Z. Lai, S. Wang, L. Lin, Y. Zhu, Y. Wang, Y. Jiang and X. Chen, *ACS Appl. Mater. Interfaces*, 2019, **11**, 26384–26391.
170 Z. Zheng, L. Liu, F. Yi and J. Zhao, *J. Lumin.*, 2019, **216**, 116722.
171 K. K. Chan, D. Giovanni, H. He, T. C. Sum and K.-T. Yong, *ACS Appl. Nano Mater.*, 2021, **4**, 9022–9033.
172 K. K. Chan, S. H. K. Yap, D. Giovanni, T. C. Sum and K.-T. Yong, *Microchem. J.*, 2022, **180**, 107624.
173 M. He, Y. Cheng, L. Shen, C. Shen, H. Zhang, W. Xiang and X. Liang, *Appl. Surf. Sci.*, 2018, **448**, 400–406.
174 J. Y. Kim, K. I. Shim, J. W. Han, J. Joo, N. H. Heo and K. Seff, *Adv. Mater.*, 2020, **32**, 2001868.
175 Y. Zhang, L. Han, B. Li and Y. Xu, *Chem. Eng. J.*, 2022, **437**, 135290.
176 J. Jiang, G. Shao, Z. Zhang, L. Ding, H. Zhang, J. Liu, Z. Chen, W. Xiang and X. Liang, *Chem. Commun.*, 2018, **54**, 12302–12305.
177 C. Shen, Y. Zhao, L. Yuan, L. Ding, Y. Chen, H. Yang, S. Liu, J. Nie, W. Xiang and X. Liang, *Chem. Eng. J.*, 2020, **382**, 122868.
178 S. Yuan, D. Chen, X. Li, J. Zhong and X. Xu, *ACS Appl. Mater. Interfaces*, 2018, **10**, 18918–18926.
179 P. Song, B. Qiao, D. Song, J. Cao, Z. Shen, G. Zhang, Z. Xu, S. Zhao, S. Wageh and A. Al-Ghamdi, *J. Mater. Sci.*, 2020, **55**, 9739–9747.
180 Z. Tan, Y. Chu, J. Chen, J. Li, G. Ji, G. Niu, L. Gao, Z. Xiao and J. Tang, *Adv. Mater.*, 2020, **32**, 2002443.
181 Z. Li, E. Hofman, J. Li, A. H. Davis, C.-H. Tung, L.-Z. Wu and W. Zheng, *Adv. Funct. Mater.*, 2018, **28**, 1704288.
182 Y. You, W. Tian, M. Wang, F. Cao, H. Sun and L. Li, *Adv. Mater. Interfaces*, 2020, **7**, 2000537.
183 G. Kang, H. Lee, J. Moon, H.-S. Jang, D.-H. Cho and D. Byun, *ACS Appl. Nano Mater.*, 2022, **5**, 6726–6735.
184 Q. Wang, Q. Dong, T. Li, A. Gruverman and J. Huang, *Adv. Mater.*, 2016, **28**, 6734–6739.
185 J. Zeng, C. Meng, X. Li, Y. Wu, S. Liu, H. Zhou, H. Wang and H. Zeng, *Adv. Funct. Mater.*, 2019, **29**, 1904461.

186 A. Pron and P. Rannou, *Prog. Polym. Sci.*, 2002, **27**, 135–190.
187 Y. Li and R. Qian, *Synth. Met.*, 1993, **53**, 149–154.
188 R. Ansari, *E-J. Chem.*, 2006, **3**, 186–201.
189 M. D. Groner, S. M. George, R. S. McLean and P. F. Carcia, *Appl. Phys. Lett.*, 2006, **88**, 051907.
190 G. Li, F. W. R. Rivarola, N. J. L. K. Davis, S. Bai, T. C. Jellicoe, F. de la Peña, S. Hou, C. Ducati, F. Gao, R. H. Friend, N. C. Greenham and Z.-K. Tan, *Adv. Mater.*, 2016, **28**, 3528–3534.
191 R. W. Johnson, A. Hultqvist and S. F. Bent, *Mater. Today*, 2014, **17**, 236–246.
192 C.-C. Shih, P.-C. Chen, G.-L. Lin, C.-W. Wang and H.-T. Chang, *ACS Nano*, 2015, **9**, 312–319.
193 S. Liu and M.-Y. Han, *Chem.–Asian J.*, 2009, **5**, 36–45.
194 A. Soleimani Dorcheh and M. H. Abbasi, *J. Mater. Process. Technol.*, 2008, **199**, 10–26.
195 H.-C. Wang, S.-Y. Lin, A.-C. Tang, B. P. Singh, H.-C. Tong, C.-Y. Chen, Y.-C. Lee, T.-L. Tsai and R.-S. Liu, *Angew. Chem., Int. Ed.*, 2016, **55**, 7924–7929.
196 M. Liu, S. Wang and L. Jiang, *Nat. Rev. Mater.*, 2017, **2**, 17036.
197 S. Wang, H. Wang, D. Zhang, Y. Dou, W. Li, F. Cao, L. Yin, L. Wang, Z.-J. Zhang, J. Zhang and X. Yang, *Chem. Eng. J.*, 2022, **437**, 135303.
198 X. Tian, T. Verho and R. H. A. Ras, *Science*, 2016, **352**, 142–143.
199 D. K. Sharma, S. Hirata and M. Vacha, *Nat. Commun.*, 2019, **10**, 4499.
200 R. H. Baney, M. Itoh, A. Sakakibara and T. Suzuki, *Chem. Rev.*, 1995, **95**, 1409–1430.
201 J. M. Newsam, *Science*, 1986, **231**, 1093–1099.
202 Y. Li and J. Yu, *Chem. Rev.*, 2014, **114**, 7268–7316.
203 V. Van Speybroeck, K. Hemelsoet, L. Joos, M. Waroquier, R. G. Bell and C. R. A. Catlow, *Chem. Soc. Rev.*, 2015, **44**, 7044–7111.
204 J.-Y. Sun, F. T. Rabouw, X.-F. Yang, X.-Y. Huang, X.-P. Jing, S. Ye and Q.-Y. Zhang, *Adv. Funct. Mater.*, 2017, **27**, 1704371.
205 G. Tong, W. Song, L. K. Ono and Y. Qi, *Appl. Phys. Lett.*, 2022, **120**, 161604.
206 J.-F. Liao, Y.-F. Xu, X.-D. Wang, H.-Y. Chen and D.-B. Kuang, *ACS Appl. Mater. Interfaces*, 2018, **10**, 42301–42309.
207 Y. Xu, X. Wang, J. Liao, B. Chen, H. Chen and D. Kuang, *Adv. Mater. Interfaces*, 2018, **5**, 1801015.
208 Y. Liu, Z. Yang, D. Cui, X. Ren, J. Sun, X. Liu, J. Zhang, Q. Wei, H. Fan, F. Yu, X. Zhang, C. Zhao and S. F. Liu, *Adv. Mater.*, 2015, **27**, 5176–5183.
209 H. Yin, J. Chen, P. Guan, D. Zheng, Q. Kong, S. Yang, P. Zhou, B. Yang, T. Pullerits and K. Han, *Angew. Chem., Int. Ed.*, 2021, **60**, 22693–22699.
210 S. Wang and X. Wang, *Small*, 2015, **11**, 3097–3112.
211 W. Lu, Z. Wei, Z.-Y. Gu, T.-F. Liu, J. Park, J. Park, J. Tian, M. Zhang, Q. Zhang, T. Gentle III, M. Bosch and H.-C. Zhou, *Chem. Soc. Rev.*, 2014, **43**, 5561–5593.
212 W. Nie and H. Tsai, *J. Mater. Chem. A*, 2022, **10**, 19518–19533.
213 D. Zhang, Y. Xu, Q. Liu and Z. Xia, *Inorg. Chem.*, 2018, **57**, 4613–4619.
214 G. Lu, S. Li, Z. Guo, O. K. Farha, B. G. Hauser, X. Qi, Y. Wang, X. Wang, S. Han, X. Liu, J. S. DuChene, H. Zhang, Q. Zhang, X. Chen, J. Ma, S. C. J. Loo, W. D. Wei, Y. Yang, J. T. Hupp and F. Huo, *Nat. Chem.*, 2012, **4**, 310–316.
215 S. Mollick, T. N. Mandal, A. Jana, S. Fajal, A. V. Desai and S. K. Ghosh, *ACS Appl. Nano Mater.*, 2019, **2**, 1333–1340.
216 S. Ahmed, S. Lahkar, S. Doley, D. Mohanta and S. Kumar Dolui, *J. Photochem. Photobiol., A*, 2023, **443**, 114821.
217 G.-Y. Qiao, D. Guan, S. Yuan, H. Rao, X. Chen, J.-A. Wang, J.-S. Qin, J.-J. Xu and J. Yu, *J. Am. Chem. Soc.*, 2021, **143**, 14253–14260.
218 Z. Xia, B. Shi, W. Zhu, Y. Xiao and C. Lü, *Adv. Funct. Mater.*, 2022, **32**, 2207655.
219 J. Hou, P. Chen, A. Shukla, A. Krajnc, T. Wang, X. Li, R. Doasa, L. H. G. Tizei, B. Chan, D. N. Johnstone, R. Lin, T. U. Schülli, I. Martens, D. Appadoo, M. S. Ari, Z. Wang, T. Wei, S. Lo, M. Lu, S. Li, E. B. Namdas, G. Mali, A. K. Cheetham, S. M. Collins, V. Chen, L. Wang and T. D. Bennett, *Science*, 2021, **374**, 621–625.
220 T. D. Bennett, Y. Yue, P. Li, A. Qiao, H. Tao, N. G. Greaves, T. Richards, G. I. Lampronti, S. A. T. Redfern, F. Blanc, O. K. Farha, J. T. Hupp, A. K. Cheetham and D. A. Keen, *J. Am. Chem. Soc.*, 2016, **138**, 3484–3492.
221 S. Horike, S. Shimomura and S. Kitagawa, *Nat. Chem.*, 2009, **1**, 695–704.
222 Y. Chen, Z. Lai, X. Zhang, Z. Fan, Q. He, C. Tan and H. Zhang, *Nat. Rev. Chem*, 2020, **4**, 243–256.
223 R. Kappera, D. Voiry, S. E. Yalcin, B. Branch, G. Gupta, A. D. Mohite and M. Chhowalla, *Nat. Mater.*, 2014, **13**, 1128–1134.
224 D. Voiry, A. Mohite and M. Chhowalla, *Chem. Soc. Rev.*, 2015, **44**, 2702–2712.
225 S. Caicedo-Dávila, H. Funk, R. Lovrinčić, C. Müller, M. Sendner, O. Cojocaru-Mirédin, F. Lehmann, R. Gunder, A. Franz, S. Levcenco, A. V. Cohen, L. Kronik, B. Haas, C. T. Koch and D. Abou-Ras, *J. Phys. Chem. C*, 2019, **123**, 17666–17677.
226 J. Hui, Y. Jiang, Ö. Ö. Gökçinar, J. Tang, Q. Yu, M. Zhang and K. Yu, *Chem. Mater.*, 2020, **32**, 4574–4583.
227 M. I. Saidaminov, M. A. Haque, J. Almutlaq, S. Sarmah, X.-H. Miao, R. Begum, A. A. Zhumekenov, I. Dursun, N. Cho, B. Murali, O. F. Mohammed, T. Wu and O. M. Bakr, *Adv. Opt. Mater.*, 2017, **5**, 1600704.
228 C. de Weerd, J. Lin, L. Gomez, Y. Fujiwara, K. Suenaga and T. Gregorkiewicz, *J. Phys. Chem. C*, 2017, **121**, 19490–19496.
229 I. Dursun, M. De Bastiani, B. Turedi, B. Alamer, A. Shkurenko, J. Yin, A. M. El-Zohry, I. Gereige, A. AlSaggaf, O. F. Mohammed, M. Eddaoudi and O. M. Bakr, *ChemSusChem*, 2017, **10**, 3746–3749.
230 M. I. Saidaminov, J. Almutlaq, S. Sarmah, I. Dursun, A. A. Zhumekenov, R. Begum, J. Pan, N. Cho, O. F. Mohammed and O. M. Bakr, *ACS Energy Lett.*, 2016, **1**, 840–845.
231 Q. A. Akkerman, T. P. T. Nguyen, S. C. Boehme, F. Montanarella, D. N. Dirin, P. Wechsler, F. Beiglböck,

G. Rainò, R. Erni, C. Katan, J. Even and M. V. Kovalenko, *Science*, 2022, **3616**, 1–13.
232 X. Zhang, B. Xu, J. Zhang, Y. Gao, Y. Zheng, K. Wang and X. W. Sun, *Adv. Funct. Mater.*, 2016, **26**, 4595–4600.
233 J. Xu, W. Huang, P. Li, D. R. Onken, C. Dun, Y. Guo, K. B. Ucer, C. Lu, H. Wang, S. M. Geyer, R. T. Williams and D. L. Carroll, *Adv. Mater.*, 2017, **29**, 1703703.
234 B. Qiao, P. Song, J. Cao, S. Zhao, Z. Shen, D. Gao, Z. Liang, Z. Xu, D. Song and X. Xu, *Nanotechnology*, 2017, **28**, 445602.
235 X. Tang, Z. Hu, W. Yuan, W. Hu, H. Shao, D. Han, J. Zheng, J. Hao, Z. Zang, J. Du, Y. Leng, L. Fang and M. Zhou, *Adv. Opt. Mater.*, 2017, **5**, 1600788.
236 Z. Ma, F. Li, G. Qi, L. Wang, C. Liu, K. Wang, G. Xiao and B. Zou, *Nanoscale*, 2019, **11**, 820–825.
237 J. Deng, J. Xun, W. Shen, M. Li and R. He, *Mater. Res. Bull.*, 2021, **140**, 111296.
238 X. Zhang, H. Wang, Y. Hu, Y. Pei, S. Wang, Z. Shi, V. L. Colvin, S. Wang, Y. Zhang and W. W. Yu, *J. Phys. Chem. Lett.*, 2019, **10**, 1750–1756.
239 J. P. McKaveney and M. D. Buck, *Anal. Chem.*, 1974, **46**, 650–654.
240 B. Zhou, Z. Liu, H. Li, S. Fang, F. Fang, Y. Wang, F. Chen and Y. Shi, *Adv. Photonics Res.*, 2021, **2**, 2100143.
241 J. Li, Z. Tan, M. Hu, C. Chen, J. Luo, S. Li, L. Gao, Z. Xiao, G. Niu and J. Tang, *Front. Optoelectron.*, 2019, **12**, 352–364.
242 Q. Ba, J. Kim, H. Im, S. Lin and A. Jana, *J. Colloid Interface Sci.*, 2022, **606**, 808–816.
243 J. You, Y. Yang, Z. Hong, T.-B. Song, L. Meng, Y. Liu, C. Jiang, H. Zhou, W.-H. Chang, G. Li and Y. Yang, *Appl. Phys. Lett.*, 2014, **105**, 183902.
244 L. Wu, H. Hu, Y. Xu, S. Jiang, M. Chen, Q. Zhong, D. Yang, Q. Liu, Y. Zhao, B. Sun, Q. Zhang and Y. Yin, *Nano Lett.*, 2017, **17**, 5799–5804.
245 M. Xie, H. Liu, F. Chun, W. Deng, C. Luo, Z. Zhu, M. Yang, Y. Li, W. Li, W. Yan and W. Yang, *Small*, 2019, **15**, 1901994.
246 A. Pramanik, S. Patibandla, Y. Gao, K. Gates and P. C. Ray, *JACS Au*, 2021, **1**, 53–65.
247 Y. Liu, F. Li, Q. Liu and Z. Xia, *Chem. Mater.*, 2018, **30**, 6922–6929.
248 S. Mamgain, V. Kunnathodi and A. Yella, *Energy Technol.*, 2020, **8**, 1900890.
249 Q. Jing, M. Zhang, X. Huang, X. Ren, P. Wang and Z. Lu, *Nanoscale*, 2017, **9**, 7391–7396.
250 K. Chen, K. Qi, T. Zhou, T. Yang, Y. Zhang, Z. Guo, C.-K. Lim, J. Zhang, I. Žutic, H. Zhang and P. N. Prasad, *Nano–Micro Lett.*, 2021, **13**, 172.
251 J. Zhu, Y. Zhu, J. Huang, L. Hou, J. Shen and C. Li, *Nanoscale*, 2020, **12**, 11842–11846.
252 F. Fang, W. Chen, Y. Li, H. Liu, M. Mei, R. Zhang, J. Hao, M. Mikita, W. Cao, R. Pan, K. Wang and X. W. Sun, *Adv. Funct. Mater.*, 2018, **28**, 1706000.
253 X. Zhang, X. Bai, H. Wu, X. Zhang, C. Sun, Y. Zhang, W. Zhang, W. Zheng, W. W. Yu and A. L. Rogach, *Angew. Chem., Int. Ed.*, 2018, **57**, 3337–3342.
254 H. Jiang, Z. Yan, H. Zhao, S. Yuan, Z. Yang, J. Li, B. Liu, T. Niu, J. Feng, Q. Wang, D. Wang, H. Yang, Z. Liu and S. F. Liu, *ACS Appl. Energy Mater.*, 2018, **1**, 900–909.
255 L. N. Quan, M. Yuan, R. Comin, O. Voznyy, E. M. Beauregard, S. Hoogland, A. Buin, A. R. Kirmani, K. Zhao, A. Amassian, D. H. Kim and E. H. Sargent, *J. Am. Chem. Soc.*, 2016, **138**, 2649–2655.
256 Y. Lin, Y. Bai, Y. Fang, Q. Wang, Y. Deng and J. Huang, *ACS Energy Lett.*, 2017, **2**, 1571–1572.
257 Y. Yang, C. Hou and T.-X. Liang, *Phys. Chem. Chem. Phys.*, 2021, **23**, 7145–7152.
258 D. Yoo, J. Y. Woo, Y. Kim, S. W. Kim, S.-H. Wei, S. Jeong and Y.-H. Kim, *J. Phys. Chem. Lett.*, 2020, **11**, 652–658.
259 A. Jana and K. S. Kim, *ACS Energy Lett.*, 2018, **3**, 2120–2126.
260 A. Jana and K. S. Kim, *ACS Appl. Energy Mater.*, 2019, **2**, 4496–4503.
261 K.-K. Liu, Q. Liu, D.-W. Yang, Y.-C. Liang, L.-Z. Sui, J.-Y. Wei, G.-W. Xue, W.-B. Zhao, X.-Y. Wu, L. Dong and C.-X. Shan, *Light: Sci. Appl.*, 2020, **9**, 44.
262 L. Jia, Z. Xu, L. Zhang, Y. Li, T. Zhao and J. Xu, *Appl. Surf. Sci.*, 2022, **592**, 153170.
263 K. Du, L. He, S. Song, J. Feng, Y. Li, M. Zhang, H. Li, C. Li and H. Zhang, *Adv. Funct. Mater.*, 2021, **31**, 2103275.
264 H. Dong, S. Kareem, X. Gong, J. Ruan, P. Gao, X. Zhou, X. Liu, X. Zhao and Y. Xie, *ACS Appl. Mater. Interfaces*, 2021, **13**, 23960–23969.
265 S. Lou, S. Si, L. Huang, W. Gan, B. Lan, J. Zhang, M. Li, T. Xuan and J. Wang, *Chem. Eng. J.*, 2022, **430**, 132680.
266 H. Lin, X. Zhang, L. Cai, J. Lao, R. Qi, C. Luo, S. Chen, H. Peng, R. Huang and C. Duan, *J. Mater. Chem. C*, 2020, **8**, 5594–5599.
267 C. Geng, S. Xu, H. Zhong, A. L. Rogach and W. Bi, *Angew. Chem., Int. Ed.*, 2018, **57**, 9650–9654.
268 P. Cheng, K. Han and J. Chen, *ACS Mater. Lett.*, 2022, 60–78.
269 X. Chen, M. Jia, W. Xu, G. Pan, J. Zhu, Y. Tian, D. Wu, X. Li and Z. Shi, *Adv. Opt. Mater.*, 2023, **11**, 2202153.
270 H. Zhao, Y. Li, B. Zhang, T. Xu and C. Wang, *Nano Energy*, 2018, **50**, 665–674.
271 H. Zhao, K. Chordiya, P. Leukkunen, A. Popov, M. Upadhyay Kahaly, K. Kordas and S. Ojala, *Nano Res.*, 2021, **14**, 1116–1125.
272 H. Wang, H. Zhang, J. Wang, Y. Gao, F. Fan, K. Wu, X. Zong and C. Li, *Angew. Chem., Int. Ed.*, 2021, **60**, 7376–7381.
273 M. Aamir, Z. H. Shah, M. Sher, A. Iqbal, N. Revaprasadu, M. A. Malik and J. Akhtar, *Mater. Sci. Semicond. Process.*, 2017, **63**, 6–11.
274 M. Becker and M. Wark, *J. Phys. Chem. C*, 2018, **122**, 3548–3557.
275 A. D'Annibale, R. Panetta, O. Tarquini, M. Colapietro, S. Quaranta, A. Cassetta, L. Barba, G. Chita and A. Latini, *Dalton Trans.*, 2019, **48**, 5397–5407.
276 X. Li, X. Zhong, Y. Hu, B. Li, Y. Sheng, Y. Zhang, C. Weng, M. Feng, H. Han and J. Wang, *J. Phys. Chem. Lett.*, 2017, **8**, 1804–1809.
277 K. Ahmad and S. M. Mobin, *Energy Technol.*, 2020, **8**, 1901185.
278 D. Ju, X. Zheng, J. Liu, Y. Chen, J. Zhang, B. Cao, H. Xiao, O. F. Mohammed, O. M. Bakr and X. Tao, *Angew. Chem., Int. Ed.*, 2018, **57**, 14868–14872.

279 D. Ju, G. Lin, H. Xiao, Y. Zhang, S. Su and J. Liu, *Sol. RRL*, 2020, **4**, 2000559.
280 M. I. Saidaminov, O. F. Mohammed and O. M. Bakr, *ACS Energy Lett.*, 2017, **2**, 889–896.
281 H. Lin, C. Zhou, Y. Tian, T. Siegrist and B. Ma, *ACS Energy Lett.*, 2018, **3**, 54–62.
282 T. Zhu and X. Gong, *InfoMat*, 2021, **3**, 1039–1069.
283 Q. Ba, A. Jana, L. Wang and K. S. Kim, *Adv. Funct. Mater.*, 2019, **29**, 1904768.
284 L. Romani, A. Bala, V. Kumar, A. Speltini, A. Milella, F. Fracassi, A. Listorti, A. Profumo and L. Malavasi, *J. Mater. Chem. C*, 2020, **8**, 9189–9194.
285 W. Bi, Z. Wang, H. Li, Y. Song, X. Liu, Y. Wang, C. Ge, A. Wang, Y. Kang, Y. Yang, B. Li and Q. Dong, *J. Phys. Chem. Lett.*, 2022, **13**, 6792–6799.
286 Z. Hong, W. K. Chong, A. Y. R. Ng, M. Li, R. Ganguly, T. C. Sum and H. Sen Soo, *Angew. Chem., Int. Ed.*, 2019, **58**, 3456–3460.
287 S.-K. Yu, Z.-R. Zhang, Z.-H. Ren, H.-L. Zhai, Q.-Y. Zhu and J. Dai, *Inorg. Chem.*, 2021, **60**, 9132–9140.
288 Z. Zhuang, C. Peng, G. Zhang, H. Yang, J. Yin and H. Fei, *Angew. Chem., Int. Ed.*, 2017, **56**, 14411–14416.
289 X. Song, G. Wei, J. Sun, C. Peng, J. Yin, X. Zhang, Y. Jiang and H. Fei, *Nat. Catal.*, 2020, **3**, 1027–1033.
290 D. Ju, G. Lin, M. Zhou, Y. Hua, X. Li, H. Li and J. Liu, *J. Mater. Chem. A*, 2022, **10**, 17752–17759.
291 C. Xue, Z.-Y. Yao, J. Zhang, W.-L. Liu, J.-L. Liu and X.-M. Ren, *Chem. Commun.*, 2018, **54**, 4321–4324.
292 X. Yang, L.-F. Ma and D. Yan, *Chem. Sci.*, 2019, **10**, 4567–4572.
293 I. Spanopoulos, I. Hadar, W. Ke, P. Guo, S. Sidhik, M. Kepenekian, J. Even, A. D. Mohite, R. D. Schaller and M. G. Kanatzidis, *J. Am. Chem. Soc.*, 2020, **142**, 9028–9038.
294 T. Sheikh, S. Maqbool, P. Mandal and A. Nag, *Angew. Chem., Int. Ed.*, 2021, **60**, 18265–18271.
295 G.-N. Liu, R.-Y. Zhao, B. Xu, Y. Sun, X.-M. Jiang, X. Hu and C. Li, *ACS Appl. Mater. Interfaces*, 2020, **12**, 54694–54702.
296 H. Peng, X. Wang, Y. Tian, T. Dong, Y. Xiao, T. Huang, Y. Guo, J. Wang and B. Zou, *J. Phys. Chem. Lett.*, 2021, **12**, 6639–6647.
297 D. A. Dougherty, *Acc. Chem. Res.*, 2013, **46**, 885–893.
298 O. M. Cabarcos, C. J. Weinheimer and J. M. Lisy, *J. Chem. Phys.*, 1998, **108**, 5151–5154.
299 Q. A. Akkerman, D. Meggiolaro, Z. Dang, F. De Angelis and L. Manna, *ACS Energy Lett.*, 2017, **2**, 2183–2186.
300 H. Liu, Z. Wu, J. Shao, D. Yao, H. Gao, Y. Liu, W. Yu, H. Zhang and B. Yang, *ACS Nano*, 2017, **11**, 2239–2247.
301 M. Lu, X. Zhang, Y. Zhang, J. Guo, X. Shen, W. W. Yu and A. L. Rogach, *Adv. Mater.*, 2018, **30**, 1804691.
302 M. Hamdan and A. K. Chandiran, *Angew. Chem., Int. Ed.*, 2020, **59**, 16033–16038.
303 Z. Xiao, H. Lei, X. Zhang, Y. Zhou, H. Hosono and T. Kamiya, *Bull. Chem. Soc. Jpn.*, 2015, **88**, 1250–1255.
304 S. Pont, D. Bryant, C.-T. Lin, N. Aristidou, S. Wheeler, X. Ma, R. Godin, S. A. Haque and J. R. Durrant, *J. Mater. Chem. A*, 2017, **5**, 9553–9560.
305 A. Aziz, N. Aristidou, X. Bu, R. J. E. Westbrook, S. A. Haque and M. S. Islam, *Chem. Mater.*, 2020, **32**, 400–409.
306 Q. Li, Z. Chen, I. Tranca, S. Gaastra-Nedea, D. Smeulders and S. Tao, *Appl. Surf. Sci.*, 2021, **538**, 148058.
307 P. Lin, A. Loganathan, I. Raifuku, M. Li, Y. Chiu, S. Chang, A. Fakharuddin, C. Lin, T. Guo, L. Schmidt-Mende and P. Chen, *Adv. Energy Mater.*, 2021, **11**, 2100818.
308 R. Babu, S. Bhandary, D. Chopra and S. P. Singh, *Chem. – Eur. J.*, 2020, **26**, 10519–10527.
309 Q. Jiang, D. Rebollar, J. Gong, E. L. Piacentino, C. Zheng and T. Xu, *Angew. Chem., Int. Ed.*, 2015, **54**, 7617–7620.
310 C.-C. Wang, J.-R. Li, X.-L. Lv, Y.-Q. Zhang and G. Guo, *Energy Environ. Sci.*, 2014, **7**, 2831–2867.
311 F. Wu, R. Pathak, J. Liu, R. Jian, T. Zhang and Q. Qiao, *ACS Appl. Mater. Interfaces*, 2021, **13**, 44274–44283.
312 A. Pisanu, A. Speltini, P. Quadrelli, G. Drera, L. Sangaletti and L. Malavasi, *J. Mater. Chem. C*, 2019, **7**, 7020–7026.
313 L. Romani, A. Speltini, F. Ambrosio, E. Mosconi, A. Profumo, M. Marelli, S. Margadonna, A. Milella, F. Fracassi, A. Listorti, F. De Angelis and L. Malavasi, *Angew. Chem., Int. Ed.*, 2021, **60**, 3611–3618.
314 L. Romani, A. Speltini, C. N. Dibenedetto, A. Listorti, F. Ambrosio, E. Mosconi, A. Simbula, M. Saba, A. Profumo, P. Quadrelli, F. De Angelis and L. Malavasi, *Adv. Funct. Mater.*, 2021, **31**, 2104428.
315 J. Liang, C. Wang, Y. Wang, Z. Xu, Z. Lu, Y. Ma, H. Zhu, Y. Hu, C. Xiao, X. Yi, G. Zhu, H. Lv, L. Ma, T. Chen, Z. Tie, Z. Jin and J. Liu, *J. Am. Chem. Soc.*, 2016, **138**, 15829–15832.
316 R. Chen, G. Gao and J. Luo, *Nano Res.*, 2022, 1–6.
317 D. Laishram, S. Zeng, K. M. Alam, A. P. Kalra, K. Cui, P. Kumar, R. K. Sharma and K. Shankar, *Appl. Surf. Sci.*, 2022, **592**, 153276.
318 M. V. Kovalenko, M. Scheele and D. V. Talapin, *Science*, 2009, **324**, 1417–1420.
319 J. Li, L. Xu, T. Wang, J. Song, J. Chen, J. Xue, Y. Dong, B. Cai, Q. Shan, B. Han and H. Zeng, *Adv. Mater.*, 2017, **29**, 1603885.
320 E. A. Muljarov, S. G. Tikhodeev, N. A. Gippius and T. Ishihara, *Phys. Rev. B: Condens. Matter Mater. Phys.*, 1995, **51**, 14370–14378.
321 H. Tsai, W. Nie, J.-C. Blancon, C. C. Stoumpos, R. Asadpour, B. Harutyunyan, A. J. Neukirch, R. Verduzco, J. J. Crochet, S. Tretiak, L. Pedesseau, J. Even, M. A. Alam, G. Gupta, J. Lou, P. M. Ajayan, M. J. Bedzyk, M. G. Kanatzidis and A. D. Mohite, *Nature*, 2016, **536**, 312–316.
322 I. C. Smith, E. T. Hoke, D. Solis-Ibarra, M. D. McGehee and H. I. Karunadasa, *Angew. Chem., Int. Ed.*, 2014, **53**, 11232–11235.
323 D. A. Hines and P. V. Kamat, *J. Phys. Chem. C*, 2013, **117**, 14418–14426.
324 W. Guan, Y. Li, Q. Zhong, H. Liu, J. Chen, H. Hu, K. Lv, J. Gong, Y. Xu, Z. Kang, M. Cao and Q. Zhang, *Nano Lett.*, 2021, **21**, 597–604.
325 Y. Wang, T. Wu, J. Barbaud, W. Kong, D. Cui, H. Chen, X. Yang and L. Han, *Science*, 2019, **365**, 687–691.

326 T. Takata, J. Jiang, Y. Sakata, M. Nakabayashi, N. Shibata, V. Nandal, K. Seki, T. Hisatomi and K. Domen, *Nature*, 2020, **581**, 411–414.
327 Y. Yang, M. Yang, D. T. Moore, Y. Yan, E. M. Miller, K. Zhu and M. C. Beard, *Nat. Energy*, 2017, **2**, 16207.
328 D. W. Wakerley, M. F. Kuehnel, K. L. Orchard, K. H. Ly, T. E. Rosser and E. Reisner, *Nat. Energy*, 2017, **2**, 17021.
329 S. Wang, B. Y. Guan and X. W. D. Lou, *J. Am. Chem. Soc.*, 2018, **140**, 5037–5040.
330 X.-D. Wang, Y.-H. Huang, J.-F. Liao, Y. Jiang, L. Zhou, X.-Y. Zhang, H.-Y. Chen and D.-B. Kuang, *J. Am. Chem. Soc.*, 2019, **141**, 13434–13441.
331 Y. Jiang, H. Chen, J. Li, J. Liao, H. Zhang, X. Wang and D. Kuang, *Adv. Funct. Mater.*, 2020, **30**, 2004293.
332 S. S. Bhosale, A. K. Kharade, E. Jokar, A. Fathi, S. Chang and E. W.-G. Diau, *J. Am. Chem. Soc.*, 2019, **141**, 20434–20442.
333 J. Sheng, Y. He, J. Li, C. Yuan, H. Huang, S. Wang, Y. Sun, Z. Wang and F. Dong, *ACS Nano*, 2020, **14**, 13103–13114.
334 J. Sheng, Y. He, M. Huang, C. Yuan, S. Wang and F. Dong, *ACS Catal.*, 2022, **12**, 2915–2926.
335 N. Li, X. Chen, J. Wang, X. Liang, L. Ma, X. Jing, D.-L. Chen and Z. Li, *ACS Nano*, 2022, **16**, 3332–3340.
336 R. Das, S. Chakraborty and S. C. Peter, *ACS Energy Lett.*, 2021, **6**, 3270–3274.
337 J. San Martin, N. Dang, E. Raulerson, M. C. Beard, J. Hartenberger and Y. Yan, *Angew. Chem., Int. Ed.*, 2022, **61**, e202205572.
338 D. Ricciarelli, W. Kaiser, E. Mosconi, J. Wiktor, M. W. Ashraf, L. Malavasi, F. Ambrosio and F. De Angelis, *ACS Energy Lett.*, 2022, **7**, 1308–1315.